

Microwave Background Signatures of a Primordial Stochastic Magnetic Field

Andrew Mack^{1†}, Tina Kahniashvili^{1,2‡}, and Arthur Kosowsky^{1,3†}

¹*Department of Physics and Astronomy, Rutgers University, 136 Frelinghuysen Road, Piscataway, New Jersey 08854-8019*

²*Center for Plasma Astrophysics, Abastumani Astrophysical Observatory, A. Kazbegi Ave. 2a, 380060 Tbilisi, Georgia*

³*School of Natural Sciences, Institute for Advanced Study, Olden Lane, Princeton, New Jersey 08540*

[†]*andymack, kosowsky@physics.rutgers.edu, [‡]tinatin@amorgos.unige.ch*

A stochastic magnetic field in the early Universe will produce anisotropies in the temperature and polarization of the cosmic microwave background. We derive analytic expressions for the microwave background temperature and polarization power spectra induced by vector and tensor perturbations from a power-law magnetic field. For a scale-invariant stochastic magnetic field smoothed over a comoving scale of 1 Mpc, the MAP satellite has the potential to constrain the comoving mean-field amplitude to be no greater than approximately 2×10^{-9} G. Limits improve as the power-law slope increases: for causally-generated power-law magnetic fields, the comoving mean-field amplitude has an upper bound of approximately 4×10^{-13} G. Such constraints will surpass all current limits on galactic-scale primordial stochastic magnetic fields at decoupling.

98.70.Vc, 98.62.En, 98.80.Cq, 98.80.Hw

I. INTRODUCTION

Magnetic fields of μG strength are ubiquitous in galaxies [1] and clusters of galaxies [2]. The origin of these fields, however, remains an outstanding problem in cosmology. It is usually postulated that these μG fields grew either via some magnetohydrodynamical (MHD) dynamo mechanism [3,4] or via adiabatic compression of a primordial magnetic field during the collapse of a protogalactic cloud [5–7]. A MHD dynamo requires tiny seed magnetic fields of comoving amplitude 10^{-20} G in conventional CDM-like cosmological models or even as tiny as 10^{-30} G in a Universe with a non-zero cosmological constant [8] as suggested by recent measurements of type Ia supernovae [9,10] and the microwave background power spectrum [11–15]. On the other hand, the adiabatic compression scenario requires a far larger primordial seed field with comoving amplitude of 10^{-9} G to 10^{-10} G.

Persistent questions about the effectiveness of MHD dynamos [16–23] together with the observation of μG magnetic fields in high-redshift galaxies [1] raise the possibility of a significant primordial magnetic field in galaxies and clusters of galaxies. The origin of such a magnetic field remains a mystery. Essentially all viable magnetogenesis mechanisms incorporate speculative ideas in high-energy theory, including (among others) inflation [24–29], electroweak [30,31] or QCD [32,33] phase transitions, charge asymmetry [34], or a ferromagnetic Yang-Mills vacuum state [35]. As the properties of the primordial magnetic field predicted varies among these mechanisms, future detections of a primordial magnetic field may aid us in identifying the correct magnetogenesis mechanism. On the cosmological front, a primordial magnetic field may have affected early-Universe processes such as phase transitions, baryogenesis, and nucleosynthesis (see [36] for a review). Relic magnetic fields could provide a direct source of information about these processes. A primordial magnetic field may also have influenced structure formation via contributing to density perturbations on galactic scales [37–40] and preserving magnetic energy in Alfvén modes on scales below the Silk damping scale during recombination [41,42]. In short, significant primordial magnetic fields would impact both cosmology and particle physics.

The presence of a magnetic field in the early Universe affects the evolution of metric perturbations, and as a result, produces temperature and polarization anisotropies in the cosmic microwave background (CMB). High-resolution measurements of the microwave background provide a clean and model-independent test for primordial magnetic fields. We demonstrate in this paper that fields large enough to result in observed fields via adiabatic compression will likely leave observable and distinctive fluctuations in the various power spectra of microwave background temperature and polarization fluctuations.

Substantial progress has been made in understanding the effects of a primordial magnetic field on the CMB. The Far Infrared Absolute Spectrophotometer (FIRAS) upper limits on chemical potential μ and Compton y distortions in the CMB blackbody constrain the present strength of the magnetic field with comoving coherence length between 400 pc and 0.6 Mpc to be $B_0 < 3 \times 10^{-8}$ G [43]. The case of a homogeneous magnetic field has been considered by several authors. The best current constraint on the primordial homogeneous magnetic field strength is $B_0 < 3.4 \times 10^{-9} (\Omega_0 h_{50}^2)^{1/2}$ G (h_{50} is the present Hubble constant in units of $50 \text{ km s}^{-1} \text{ Mpc}^{-1}$), obtained by doing statistical analysis on the 4-year Cosmic Background Explorer (COBE) data for temperature patterns of a Bianchi type VII anisotropic spacetime [44]. A primordial homogeneous magnetic field can produce distortions of the CMB

acoustic peaks via fast magnetosonic waves [45]; meanwhile, Alfvén wave excitations can amplify vector perturbations and induce additional correlations in temperature multipole moments [46]. It is shown in Ref. [47] that a primordial homogeneous magnetic field of present strength 10^{-9} G at decoupling can induce a measurable Faraday rotation in the CMB polarization of 1° at a frequency of 30 GHz. Additional CMB polarization effects arising from a primordial homogeneous magnetic field via Faraday rotation include a parity-odd cross correlation between temperature and polarization anisotropies [48] and the depolarization of the original CMB polarization [49], which leads to a reduction in the damping of temperature anisotropies on small angular scales.

The case of a stochastic magnetic field is perhaps more realistic, because such fields are observed within galaxy clusters [50–53] and predicted by all causal magnetogenesis mechanisms [36]. Some numerical estimates of CMB temperature and polarization power spectra from density perturbations induced by a primordial stochastic magnetic field are presented in Ref. [54], whereas corresponding analytic estimates, though somewhat crude and valid only for temperature anisotropies on large angular scales, are given in Ref. [55]. Effects of Alfvén waves induced by a primordial stochastic magnetic field on CMB temperature and B-type polarization anisotropies are considered in Refs. [56] and [57] respectively. Finally, a primordial stochastic magnetic field also generates gravitational waves; the resulting tensor CMB temperature power spectrum is given in Ref. [58].

Although a variety of effects of a primordial stochastic magnetic field on the CMB have been investigated, the results are fragmented and a systematic approach is lacking. Besides the temperature power spectrum from tensor perturbations given in Ref. [58], no other CMB power spectra have been derived. We consider a statistically homogeneous and isotropic stochastic magnetic field with a power-law power spectrum, generated at some early epoch of the radiation-dominated Universe. Based on the computational techniques in Ref. [58] and the total angular momentum method for calculating CMB anisotropies introduced by Hu and White [59], we have completed a comprehensive and unified analytic calculation of all types of CMB power spectra arising from a primordial stochastic magnetic field. This paper focuses on the induced vector and tensor perturbations. A primordial magnetic field acts as a continuous source of vorticity until decoupling and gravitational radiation until matter-radiation equality. The resulting vector and tensor perturbations are one of the few cosmological sources of B-type polarization [60,61], along with primordial tensor perturbations [62] and gravitational lensing of the CMB [63]. Scalar perturbations induce CMB anisotropies smaller than those from vector and tensor perturbations and hence will not be considered here (see Sec. VIII).

In Sec. II we derive the power spectrum for a primordial stochastic magnetic field. We then project the vector and tensor pieces from the electromagnetic stress-energy tensor, from which we calculate their two-point correlation functions and derive their isotropic spectra. Details of the derivation of the vector isotropic spectrum are presented in the Appendix. Section III computes the magnetic damping scales of the induced vector perturbations at decoupling and tensor perturbations at matter-radiation equality. In Sec. IV we review the vector and tensor contributions to the metric tensor and give their corresponding evolution equations. We obtain solutions to these equations, which can be expressed as functions of the magnetic-induced isotropic spectra derived in Sec. II. Using the total angular momentum method of Ref. [59], we compute analytically the CMB power spectra for temperature in Sec. V, polarization in Sec. VI, and the temperature-polarization cross correlation in Sec. VII. Section VIII concludes with the physical interpretation of these results and a discussion of current and future limits on primordial magnetic fields from the microwave background. For the vector perturbations, the B-type is slightly larger than the E-type polarization power spectrum, whereas the E-type polarization and the cross-correlation power spectra are approximately identical. For the tensor perturbations, the polarization power spectra are actually comparable to the temperature power spectrum for $n > -3/2$, where n is the magnetic field power-law spectral index. As we will show in Sec. III, the tensor perturbations are damped on smaller scales than the vector perturbations. The magnetic cutoff wavenumber determines the overall amplitude of the CMB power spectra, so the tensor-induced CMB anisotropies will be larger than the vector anisotropies for $n > -3/2$. For a scale-invariant stochastic magnetic field smoothed over a comoving scale of 1 Mpc, near-future microwave background temperature measurements will constrain the comoving mean-field amplitude to be no greater than approximately 2×10^{-9} G. Limits improve as n increases: for causally-generated power-law magnetic fields with $n \geq 2$, the comoving mean-field amplitude will soon have an upper bound of approximately 4×10^{-13} G. These will be the strongest current constraints on galactic-scale primordial stochastic magnetic fields at decoupling. Eventually, precision measurements of the microwave background temperature and polarization will give significantly stronger constraints.

In this paper, we focus on the induced CMB anisotropies for $l \leq 500$, where the analysis is relatively clean, simple, and free from complications arising from the last-scattering microphysics. For simplicity, we consider the case of a flat Universe with a vanishing cosmological constant. We employ the following notational conventions: a is the scale factor, η is the conformal time, overdots are derivatives with respect to η , and 0 subscripts denote the present time. We set $c = 1$ and normalize the scale factor to unity today. As usual, Greek indices run from 0 to 3 and Latin ones from 1 to 3. All calculations are done in Fourier space, unless real-space dependence is indicated explicitly (as in Sec. II). All magnetic field amplitudes are comoving values, unless an explicit time dependence is displayed.

II. MAGNETIC POWER SPECTRUM AND CORRELATION FUNCTIONS

Consider a primordial stochastic magnetic field created at some specific moment during the radiation-dominated epoch. The energy density of the magnetic field is treated as a first-order perturbation to a flat Friedmann-Robertson-Walker (FRW) background cosmology. In other words, we do not decompose the magnetic field into a large homogeneous component and a small fluctuating piece as in most cases in the literature. Within the linear approximation, the magnetic field evolves as a stiff source and we discard all MHD fluid back reactions onto the field itself [58]. Prior to decoupling, the conductivity of the primordial plasma is very large [24,64] and for practical purposes can be assumed infinite. In the comoving frame, this implies the “frozen-in” condition $\mathbf{E} = -\mathbf{v} \times \mathbf{B}$, where \mathbf{v} is the plasma peculiar velocity and \mathbf{E} is the electric field induced by plasma motions. Infinite conductivity leads to a vanishing electric field in linear perturbation theory ($v \ll 1$) and allows the time evolution of the magnetic field to decouple from its spatial structure on sufficiently large scales. As the Universe expands, magnetic field lines are simply conformally diluted due to flux conservation: $\mathbf{B}(\eta, \mathbf{x}) = \mathbf{B}(\mathbf{x})/a^2$. On small scales, however, a primordial magnetic field is damped due to photon and neutrino viscosities [41,42]. As in Ref. [58], we parametrize this damping by introducing a hard ultraviolet cutoff wavenumber k_D in the magnetic power spectrum. We will compute the magnetic damping cutoff wavenumbers k_D 's for both vector and tensor perturbations in Sec. III.

A statistically homogeneous and isotropic magnetic field must have the two-point correlation function [58,65]

$$\langle B_i(\mathbf{k})B_j^*(\mathbf{k}') \rangle = (2\pi)^3 P_{ij} P(k) \delta(\mathbf{k} - \mathbf{k}'), \quad (2.1)$$

where

$$P_{ij} \equiv \delta_{ij} - \hat{k}_i \hat{k}_j \quad (2.2)$$

is a projector onto the transverse plane:

$$P_{ij} P_{jk} = P_{ik}, \quad P_{ij} \hat{k}_j = 0, \quad (2.3)$$

and $\hat{k}_i = k_i/k$. We adopt the Fourier transform convention

$$B_i(\mathbf{k}) = \int d^3x \exp(i\mathbf{k} \cdot \mathbf{x}) B_i(\mathbf{x}). \quad (2.4)$$

Note the projection tensor of Eq. (2.2) is valid only for the case of a flat Universe where perturbations can be decomposed into plane waves; for non-zero spatial curvatures, the analog to a plane-wave basis must be employed (see, e.g., [66]). A specific magnetogenesis model consists of specifying the function $P(k)$, which we take to be a power law

$$P(k) = Ak^n. \quad (2.5)$$

Our primary interest is to constrain the primordial comoving magnetic field strength on a certain comoving length scale. We therefore convolve the field with a 3D-Gaussian filter transform of comoving radius λ , $B_i(\mathbf{k}) \rightarrow B_i(\mathbf{k}) * f_k$, where $f_k = \exp(-\lambda^2 k^2/2)$, and normalize as

$$\langle B_i(\mathbf{x})B_i(\mathbf{x}) \rangle |_\lambda = B_\lambda^2. \quad (2.6)$$

Thus B_λ is the magnetic comoving mean-field amplitude obtained by smoothing over a Gaussian sphere of comoving radius λ . The corresponding mean-square value B_λ^2 is then given by the Fourier transform of the product of the power spectrum $P(k)$ and the square of the filter transform f_k ,

$$B_\lambda^2 = \frac{2}{(2\pi)^3} \int d^3k P(k) |f_k|^2 \simeq \frac{2A}{(2\pi)^2} \frac{1}{\lambda^{n+3}} \Gamma\left(\frac{n+3}{2}\right), \quad (2.7)$$

with the factor 2 coming from the trace of the projection tensor of Eq. (2.2). We require the spectral index $n > -3$ to prevent infrared divergence of the integral over the spectrum of long wavelengths $k \rightarrow 0$. Solving for the normalization constant A and using Eqs. (2.1) and (2.5), we arrive at the two-point correlation function for a primordial stochastic magnetic field

$$\langle B_i(\mathbf{k})B_j^*(\mathbf{k}') \rangle = \frac{(2\pi)^{n+8}}{2} \frac{B_\lambda^2}{\Gamma\left(\frac{n+3}{2}\right)} P_{ij} \frac{k^n}{k_\lambda^{n+3}} \delta(\mathbf{k} - \mathbf{k}'), \quad k < k_D, \quad (2.8)$$

where $k_\lambda = 2\pi/\lambda$. The spectrum vanishes for all scales smaller than the damping scale $k > k_D$. The condition $n > -3$ guarantees that superhorizon coherent fields are not overproduced; the limit $n \rightarrow -3$ approaches a scale-invariant spectrum. The case $n = 0$ corresponds to a white noise spectrum where we have equal power at all wavelengths. For a causally-generated stochastic magnetic field, we require $n \geq 2$ [58,65,67].

The induced electromagnetic stress-energy tensor is given by the convolution of the magnetic field [68]

$$\tau_{ij}^{(B)}(\mathbf{k}) = \frac{1}{(2\pi)^3} \frac{1}{4\pi} \int d^3p \left[B_i(\mathbf{p})B_j(\mathbf{k}-\mathbf{p}) - \frac{1}{2}\delta_{ij}B_l(\mathbf{p})B_l(\mathbf{k}-\mathbf{p}) \right]. \quad (2.9)$$

It can be geometrically decomposed into scalar, vector, and tensor perturbation modes, $\tau_{ij}^{(B)} = \Pi_{ij}^{(S)} + \Pi_{ij}^{(V)} + \Pi_{ij}^{(T)}$, according to their three-space coordinate transformation properties on the constant-time hypersurface [69]. In the linear approximation, all types of cosmological perturbations are decoupled from each other dynamically; thus we can consider each type of perturbation independently. From the tensor $\Pi_{ij}^{(V)}$ we can construct a vector $\Pi_i^{(V)}$ that sources the vorticity perturbations, whereas the tensor $\Pi_{ij}^{(T)}$ sources the gravitational wave perturbations. To obtain CMB power spectra, we need to derive two-point correlation functions for $\Pi_i^{(V)}$ and $\Pi_{ij}^{(T)}$ and extract their corresponding isotropic spectra $|\Pi^{(V),(T)}(k)|^2$. This is the subject to which we now turn.

A. Vector Projection and Correlation Function

We begin by illustrating how to project from a generic spatial metric perturbation δg_{ij} its vector piece $\delta g_{ij}^{(V)}$. A vector spatial metric perturbation must have the form [69]

$$\delta g_{ij}^{(V)} = \xi_i \hat{k}_j + \xi_j \hat{k}_i, \quad (2.10)$$

where ξ_i is a divergenceless three vector. A possible construction for ξ_i is given by

$$\xi_i = \hat{k}_m \delta g_{mi} - \hat{k}_i \hat{k}_m \hat{k}_n \delta g_{mn}. \quad (2.11)$$

The projection then follows from substituting Eq. (2.11) into Eq. (2.10):

$$\delta g_{ij}^{(V)} = (\hat{k}_m \delta g_{mi} - \hat{k}_i \hat{k}_m \hat{k}_n \delta g_{mn}) \hat{k}_j + (\hat{k}_m \delta g_{mj} - \hat{k}_j \hat{k}_m \hat{k}_n \delta g_{mn}) \hat{k}_i = (P_{in} \hat{k}_j + P_{jn} \hat{k}_i) \hat{k}_m \delta g_{mn}. \quad (2.12)$$

Using Eq. (2.12), the vector part of the electromagnetic stress-energy tensor is given by

$$\Pi_{ij}^{(V)} = (P_{in} \hat{k}_j + P_{jn} \hat{k}_i) \hat{k}_m \tau_{mn}^{(B)}, \quad (2.13)$$

from which we can construct a vector $\Pi_i^{(V)}$ via contracting with the unit vector \hat{k}_j ,

$$\Pi_i^{(V)} = \Pi_{ij}^{(V)} \hat{k}_j = P_{in} \hat{k}_m \tau_{mn}^{(B)}. \quad (2.14)$$

The physical meaning of $\Pi_i^{(V)}$ is clear upon examining the Lorentz force vector. In the infinite conductivity limit, the Lorentz force vector in real space is given by [55,68]

$$\mathbf{L}(\mathbf{x}) \simeq -\frac{1}{4\pi} \{ \mathbf{B}(\mathbf{x}) \times [\nabla \times \mathbf{B}(\mathbf{x})] \} = \frac{1}{4\pi} \left\{ [\mathbf{B}(\mathbf{x}) \cdot \nabla] \mathbf{B}(\mathbf{x}) - \frac{1}{2} \nabla B^2(x) \right\}. \quad (2.15)$$

Fourier transforming Eq. (2.15), extracting the corresponding vortical component $L_i^{(V)}$ which satisfies the divergenceless condition $L_i^{(V)} \hat{k}_i = 0$, and comparing with Eq. (2.14) shows that

$$L_i^{(V)} = k \Pi_i^{(V)}. \quad (2.16)$$

The vector $\Pi_i^{(V)}$ will appear in the evolution equations for vector perturbations in Sec. IV A.

The stochastic and transverse nature of $\Pi_i^{(V)}$ lead us to define the two-point correlation function

$$\langle \Pi_i^{(V)}(\mathbf{k}) \Pi_j^{(V)*}(\mathbf{k}') \rangle \equiv P_{ij} |\Pi^{(V)}(k)|^2 \delta(\mathbf{k} - \mathbf{k}'). \quad (2.17)$$

The vector isotropic spectrum $|\Pi^{(V)}(k)|^2$ can be obtained using Eq. (2.14) for $\Pi_i^{(V)}$, evaluating the two-point correlation function of the electromagnetic stress-energy tensor of Eq. (2.9), and comparing the result with Eq. (2.17). A lengthy calculation in the Appendix gives

$$|\Pi^{(V)}(k)|^2 \simeq \frac{1}{8\pi(2n+3)} \left[\frac{(2\pi)^{n+5} B_\lambda^2}{2\Gamma\left(\frac{n+3}{2}\right) k_\lambda^{n+3}} \right]^2 \left(k_D^{2n+3} + \frac{n}{n+3} k^{2n+3} \right), \quad k < k_D. \quad (2.18)$$

The first term dominates when $n > -3/2$, whereas the second term dominates when $-3 < n < -3/2$. For the case $n > -3/2$, the vector isotropic spectrum becomes approximately white noise (independent of k) and depends on the ultraviolet cutoff wavenumber k_D . This is because the induced electromagnetic stress-energy tensor of Eq. (2.9) is quadratic in the stochastic magnetic field and the convolution of the magnetic field couples the large and small scale modes. Each mode of the vector isotropic spectrum is then affected by all scales of the magnetic power spectrum of Eq. (2.8) and for the case of $n > -3/2$, the cutoff scale perturbations completely dominate the large scale modes (see also Sec. V of Ref. [58]). Note that the term within the square bracket is the normalization A of the magnetic power spectrum in Eq. (2.5). To simplify the calculation, we will only consider the corresponding dominant term for a given spectral index n , although including the contributions from both terms is a straightforward extension of the calculation presented here. In the neighborhood of $n = -3/2$, both terms must be included to handle correctly the removable singularity.

B. Tensor Projection and Correlation Function

Gravitational radiation is produced by the transverse and traceless piece of the electromagnetic stress-energy tensor, given by (see, e.g., [58])

$$\Pi_{ij}^{(T)} = (P_{im}P_{jn} - \frac{1}{2}P_{ij}P_{mn})\tau_{mn}^{(B)}. \quad (2.19)$$

It follows from the transverse and traceless properties of the tensor $\Pi_{ij}^{(T)}$ that its two-point correlation function can be written as [58]

$$\langle \Pi_{ij}^{(T)}(\mathbf{k}) \Pi_{lm}^{(T)*}(\mathbf{k}') \rangle \equiv \mathcal{M}_{ijlm} |\Pi^{(T)}(k)|^2 \delta(\mathbf{k} - \mathbf{k}'). \quad (2.20)$$

The tensor structure \mathcal{M}_{ijlm} is

$$\begin{aligned} \mathcal{M}_{ijlm} &\equiv P_{il}P_{jm} + P_{im}P_{jl} - P_{ij}P_{lm} \\ &= \delta_{il}\delta_{jm} + \delta_{im}\delta_{jl} - \delta_{ij}\delta_{lm} + \hat{k}_i\hat{k}_j\hat{k}_l\hat{k}_m \\ &\quad + \delta_{ij}\hat{k}_l\hat{k}_m + \delta_{lm}\hat{k}_i\hat{k}_j - \delta_{il}\hat{k}_j\hat{k}_m - \delta_{jm}\hat{k}_i\hat{k}_l - \delta_{im}\hat{k}_j\hat{k}_l - \delta_{jl}\hat{k}_i\hat{k}_m \end{aligned} \quad (2.21)$$

and satisfies $\mathcal{M}_{ijji} = 4$ and $\mathcal{M}_{iilm} = \mathcal{M}_{ijll} = 0$. The tensor isotropic spectrum $|\Pi^{(T)}(k)|^2$ can be obtained using Eq. (2.19) for $\Pi_{ij}^{(T)}$, evaluating the two-point correlation function of the electromagnetic stress-energy tensor of Eq. (2.9), and comparing the result with Eq. (2.20). A similar calculation as in the case of the vector isotropic spectrum gives

$$|\Pi^{(T)}(k)|^2 \simeq \frac{1}{16\pi(2n+3)} \left[\frac{(2\pi)^{n+5} B_\lambda^2}{2\Gamma\left(\frac{n+3}{2}\right) k_\lambda^{n+3}} \right]^2 \left(k_D^{2n+3} + \frac{n}{n+3} k^{2n+3} \right), \quad k < k_D. \quad (2.22)$$

The tensor isotropic spectrum differs from its vector counterpart only by a factor of two, due to the ratio of traces of their corresponding tensor structures P_{ij} and \mathcal{M}_{ijlm} . Again, the first term dominates when $n > -3/2$, whereas the second term dominates when $-3 < n < -3/2$. For the case of $n > -3/2$, the cutoff scale perturbations completely dominate the large scale modes and hence the tensor isotropic spectrum depends on the ultraviolet cutoff wavenumber k_D ; the resulting tensor CMB temperature power spectrum then possesses the well-known behavior of a white noise source, $l^2 C_l \propto l^3$ [58]. We will demonstrate that this is also true for tensor CMB polarization and temperature-polarization cross correlation. As above, the term within the square bracket is the normalization A of the magnetic power spectrum in Eq. (2.5). As with the vector case, we will only consider the dominant term of Eq. (2.22) for a given spectral index n .

III. MAGNETIC DAMPING SCALES

The evolution and damping of primordial magnetic fields are studied in Refs. [41,42]. These authors consider cases for which either the magnetic field is linearized about a constant background field [41] or a magnetic field with a tangled component of unrestricted amplitude is superposed perpendicularly on a homogeneous field [42]. We are interested in a stochastic magnetic field with a power-law power spectrum. We will first briefly recapitulate the findings of Refs. [41,42]. Based on these results, we then proceed to compute the magnetic damping scales separately for vector and tensor perturbations for a power-law magnetic field.

Primordial magnetic fields are damped by radiative viscosity, which arises from the finite mean free paths of neutrinos and photons. Damping of MHD modes by neutrino viscosity is the most efficient around neutrino decoupling ($T \sim 1$ MeV). At that time, the neutrino physical mean free path ($l_{\nu \text{ dec}} \approx 10^{11}$ cm) and the Hubble length ($H_{\nu \text{ dec}}^{-1} \approx 5 \times 10^{10}$ cm) are comparable, hence the dissipation of magnetic energy can only occur on relatively small scales. Photon viscosity, on the other hand, damps MHD modes from after e^+e^- annihilation ($T \sim 20$ keV) until recombination ($T \sim 0.25$ eV); thus it is capable of dissipating magnetic energy on larger scales. There are three types of propagating MHD modes: fast and slow magnetosonic waves, with the fluid velocity making an arbitrary angle with the background magnetic field; and Alfvén waves, with the fluid velocity oriented perpendicular to the wave vector \mathbf{k} and the background magnetic field. Alfvén waves induce neither density nor temperature perturbations. Fast magnetosonic waves are similar in nature to sound waves. Like the acoustically oscillating density fluctuations, they are Silk-damped by radiation diffusion on scales below the radiation diffusion length. Meanwhile, slow magnetosonic and Alfvén waves possess similar behaviors. During the radiation diffusion regime ($k_{\text{phys}}^{-1} > l_{\nu, \gamma}$), these waves either oscillate negligibly or become overdamped, hence the dissipation of magnetic energy becomes inefficient. It is only upon entering the free-streaming regime ($k_{\text{phys}}^{-1} < l_{\nu, \gamma}$) before recombination that these waves will suffer additional damping. The resulting maximum damping scale for these waves is dependent on the background magnetic field strength and is on the order of the Alfvén velocity times the comoving Silk scale. Since Alfvén modes describe incompressible motions, we can obtain the magnetic damping scales for vector and tensor perturbations via computing the damping scales of such modes for a power-law magnetic power spectrum.

A. Vector Perturbations

Since vector perturbations induce CMB anisotropies via vorticity at recombination, we need to evaluate the Alfvén wave damping scales at recombination for a power-law magnetic field. Around recombination, all Alfvén modes are overdamped. The modes that suffer the most damping while overdamped are those in the free-streaming regime [41,42]. For a non-linear Alfvén mode propagating in a uniform background field $\bar{\mathbf{B}}$, its free-streaming damping scale at recombination is given by Eq. (8.11) of Ref. [42]:

$$k_D^{-1} = \frac{\lambda_D}{2\pi} \approx \sqrt{\frac{3}{5}} V_A L_S \approx 5.7 \times 10^{-3} \left(\frac{\bar{B}}{10^{-9} \text{ G}} \right) h^{-1/2} \text{ Mpc}, \quad (3.1)$$

where L_S is the comoving Silk scale at recombination and we have assumed $T_{\text{dec}} = 0.25$ eV, $\Omega_b h^2 = 0.0125$, and a matter-dominated Universe at recombination. The Alfvén velocity V_A arises from the uniform background field $\bar{\mathbf{B}}$. For a linearized Alfvén mode, we have to replace V_A by $V_A \cos \theta$, where θ is the angle between the wave vector and the zero-order background field (cf. Eq. (108) of Ref. [41]).

For a stochastic magnetic field with a power-law power spectrum, the effective homogeneous magnetic field responsible for the Alfvén velocity can be obtained via smoothing the stochastic field. As in Ref. [57], we assume the field smoothed over the damping scale λ_D acts as the effective homogeneous field \bar{B}_{eff} . For each spectral index n , $B_\lambda^2 \propto \lambda^{-(n+3)}$ [cf. Eq. (2.7)], and \bar{B}_{eff} is related to B_λ through (see also Eq. (26) of Ref. [58])

$$\bar{B}_{\text{eff}} = B_\lambda \left(\frac{k_D}{k_\lambda} \right)^{\frac{n+3}{2}}. \quad (3.2)$$

Smoothing the stochastic magnetic field on scales larger than the damping scale will result in a smaller effective homogeneous field, hence a smaller effective Alfvén velocity and a larger momentum cutoff wavenumber k_D . Since for $n > -3/2$ the vorticity source becomes approximately white noise (independent of k) and is k_D -dependent [cf. Eq. (2.18)], a larger momentum cutoff wavenumber k_D will give rise to larger CMB anisotropies in this regime as we will see. The estimation in Eq. (3.2) is therefore a conservative one. Substituting Eq. (3.2) into (3.1) yields

$$k_D \approx (1.7 \times 10^2)^{\frac{2}{n+5}} \left(\frac{B_\lambda}{10^{-9} \text{G}} \right)^{-\frac{2}{n+5}} \left(\frac{k_\lambda}{1 \text{Mpc}^{-1}} \right)^{\frac{n+3}{n+5}} h^{\frac{1}{n+5}} \text{Mpc}^{-1}. \quad (3.3)$$

Note that for a given spectral index n , $B_\lambda^2/k_\lambda^{n+3} \propto A$, where A is the normalization of the magnetic power spectrum in Eq. (2.5).

B. Tensor Perturbations

Since the sourcing of gravitational radiation after the Universe becomes matter-dominated is negligible (see Sec. IV B and also Ref. [58]), the relevant tensor damping scales are the Alfvén wave damping scales at equality. As in recombination, all Alfvén modes are also overdamped around equality, hence the modes that are undergoing free streaming suffer the most damping. The situation is clearly depicted in Fig. 1 of Ref. [41]. The Alfvén wave free-streaming damping scale at equality is (cf. Eq. (106) of Ref. [41] and Eq. (8.10) of Ref. [42])

$$k_D^{-1} = \frac{\lambda_D}{2\pi} \approx \sqrt{\frac{3}{5}} V_A L_\gamma^{\text{diff}}(T_{\text{eq}}), \quad (3.4)$$

where $L_\gamma^{\text{diff}}(T_{\text{eq}})$ is the photon comoving diffusion length at equality,

$$\begin{aligned} L_\gamma^{\text{diff}}(T_{\text{eq}}) &\approx 19.5 \left(\frac{T_{\text{eq}}}{0.25 \text{eV}} \right)^{-5/4} h^{-1/2} \left(\frac{\Omega_b h^2}{0.0125} \right)^{-1/2} \text{Mpc} \\ &\approx 0.41 h^{-3} \text{Mpc}, \end{aligned} \quad (3.5)$$

assuming $T_{\text{eq}} = 5.5 \text{eV}(\Omega_0 h^2)$, $\Omega_0 = 1$, and $\Omega_b h^2 = 0.0125$. Substituting Eq. (3.5) into (3.4), a similar manipulation as in the case of vector perturbations gives

$$k_D \approx (8.3 \times 10^3)^{\frac{2}{n+5}} \left(\frac{B_\lambda}{10^{-9} \text{G}} \right)^{-\frac{2}{n+5}} \left(\frac{k_\lambda}{1 \text{Mpc}^{-1}} \right)^{\frac{n+3}{n+5}} h^{\frac{6}{n+5}} \text{Mpc}^{-1}. \quad (3.6)$$

Note again that for a given spectral index n , $B_\lambda^2/k_\lambda^{n+3} \propto A$, where A is the normalization of the magnetic power spectrum in Eq. (2.5).

Several comments are in order. First, since the tensor source contributes earlier (at equality) than the vector source (at recombination), tensor perturbations are damped at smaller scales as illustrated by Eqs. (3.3) and (3.6). For $n > -3/2$, CMB power spectra are dependent on the momentum cutoff wavenumber k_D and scale with it as k_D^{2n+3} , we therefore expect tensor perturbations to generate larger anisotropies than the vector perturbations in this regime, at least for $l \leq 500$ that we are considering. Second, in Ref. [58], the magnetic damping cutoff wavenumber for tensor perturbations is found to be 4.5Mpc^{-1} . This value is derived based on the assumption that the Alfvén modes are undergoing damped oscillatory motions. Our analysis however, shows that for the magnetic field strengths considered here, the Alfvén modes should be in the overdamped free-streaming regime around equality, as also illustrated in Fig. 1 of Ref. [41]. Finally, as pointed out in Ref. [41], the Alfvén damping scale at equality could in principle be larger than that given by Eq. (3.4) since additional damping could arise due to a possible breakdown of the WKB approximation in the regime where the Alfvén mode is undergoing overdamped free streaming. In the absence of an accurate quantitative treatment for Alfvén damping scales in this regime, Eq. (3.4) is our best-educated guess. Nevertheless, we caution the readers that with a possible larger damping scale k_D^{-1} than that given by Eq. (3.4), the induced tensor anisotropies for $n > -3/2$ will be reduced accordingly.

IV. METRIC PERTURBATIONS AND THEIR EVOLUTION

A primordial stochastic magnetic field generates CMB anisotropies via its gravitational effects on the metric tensor. The full metric tensor can be decomposed into its background and perturbation pieces, $g_{\mu\nu} = g_{\mu\nu}^{(0)} + \delta g_{\mu\nu}$; for a flat Universe with the usual conformal FRW metric, $g_{\mu\nu}^{(0)} = a^2 \eta_{\mu\nu}$, where $\eta_{\mu\nu} = \text{diag}(-1, 1, 1, 1)$ is the Minkowski metric tensor. The vector (Sec. IV A) and tensor (Sec. IV B) perturbations are calculated separately; scalar perturbations will generally result in smaller CMB anisotropies compared to vector and tensor contributions, as argued in Sec. VIII, and so will not be considered here. We review the various metric tensor contributions and give the corresponding evolution equations due to a primordial stochastic magnetic field. We then obtain solutions to these equations, which can be expressed as functions of the isotropic spectra derived in Sec. II.

A. Vector Perturbations

Vector perturbations to the geometry are described by two divergenceless three-vectors ζ_i and ξ_i with the general form [see Eq. (2.10) also]

$$\delta g_{0i}^{(V)} = -a^2 \zeta_i, \quad \delta g_{ij}^{(V)} = a^2 (\xi_i \hat{k}_j + \xi_j \hat{k}_i). \quad (4.1)$$

Vector perturbations represent vorticity; the divergenceless condition for vectors ζ_i and ξ_i guarantees the absence of density perturbations. Vector perturbations exhibit gauge freedom, which arises because the mapping of coordinates between the perturbed physical manifold and the background is not unique. From vectors ζ_i and ξ_i , we can construct a gauge-invariant vector potential $V_i = \zeta_i + \dot{\xi}_i/k$ that geometrically describes the vector perturbations of the extrinsic curvature [70,71]. We now exploit the gauge freedom by explicitly choosing ξ_i to be a constant vector in time; it follows that $\delta g_{0i}^{(V)} = -a^2 V_i$. Vector perturbations of the stress-energy tensor can be parametrized by a divergenceless three-vector $\mathbf{v}^{(V)}$ that perturbs the four-velocity $u_\mu = (1, 0, 0, 0)$ of a stationary fluid element in the comoving frame [46]:

$$\delta u_\mu = (0, \mathbf{v}^{(V)}/a). \quad (4.2)$$

We can now construct a gauge-invariant, divergenceless three-vector termed the ‘‘vorticity,’’

$$\Omega_i = v_i^{(V)} - V_i. \quad (4.3)$$

Two Einstein equations govern vector perturbation evolution. The first describes the vector potential evolution under the influence of a primordial stochastic magnetic field:

$$\dot{V}_i(\eta, \mathbf{k}) + 2\frac{\dot{a}}{a}V_i(\eta, \mathbf{k}) = -\frac{16\pi G\Pi_i^{(V)}(\mathbf{k})}{a^2k}, \quad (4.4)$$

where $\Pi_i^{(V)}(\mathbf{k})$ is given by Eq. (2.14) and we neglect the vector anisotropic stress of the plasma, which is in general negligible. The magnetic field source terms $\Pi_i^{(V)}(\mathbf{k})$ and $\Pi_{ij}^{(T)}(\mathbf{k})$ are expressed in terms of present comoving magnetic field amplitudes. Since both of these terms depend on the magnetic field quadratically, the explicit time dependence of the magnetic stress is given by $\Pi(\eta, \mathbf{k}) = \Pi(\mathbf{k})/a^4$. In the absence of the magnetic source term, the homogeneous solution of this equation behaves like $V_i \propto 1/a^2$. The complete solution including the magnetic source is simply

$$V_i(\eta, \mathbf{k}) = -\frac{16\pi G\Pi_i^{(V)}(\mathbf{k})\eta}{a^2k}. \quad (4.5)$$

During the radiation-dominated epoch we have $a \propto \eta$; a magnetic field therefore causes vector perturbations to decay less rapidly ($1/a$ instead of $1/a^2$) with the Universe’s expansion. The second vector Einstein equation is a constraint that relates the vector potential to the vorticity:

$$-k^2 V_i(\eta, \mathbf{k}) = 16\pi G a^2 (\rho + p) \Omega_i(\eta, \mathbf{k}). \quad (4.6)$$

Vector conservation equations can be obtained via covariant conservation of the stress-energy tensor. Since vector perturbations cannot generate density perturbations, we have

$$\delta_\gamma = \delta_b = 0. \quad (4.7)$$

Before decoupling, photons are coupled to baryons via Thomson scattering. The magnetic field affects the photon-baryon fluid dynamics via the baryons; we therefore introduce the Lorentz force term into the baryon Euler equation. The Euler equations for photons and baryons are respectively [55,59]

$$\dot{\Omega}_{\gamma i} + \dot{\tau}(v_{\gamma i}^{(V)} - v_{bi}^{(V)}) = 0, \quad (4.8)$$

$$\dot{\Omega}_{bi} + \frac{\dot{a}}{a}\Omega_{bi} - \frac{\dot{\tau}}{R}(v_{\gamma i}^{(V)} - v_{bi}^{(V)}) = \frac{L_i^{(V)}(\mathbf{k})}{a^4(\rho_b + p_b)}. \quad (4.9)$$

In the above, $\Omega_{\gamma,b} = \mathbf{v}_{\gamma,b}^{(V)} - \mathbf{V}$ represent vorticities of photons and baryons; $\dot{\tau} = n_e \sigma_T a$ is the differential optical depth where n_e is the free electron density and σ_T is the Thomson cross section; $R \equiv (\rho_b + p_b)/(\rho_\gamma + p_\gamma) \simeq 3\rho_b/4\rho_\gamma$ is the

momentum density ratio between baryons and photons; and $L_i^{(V)}$ is the vortical piece of the Lorentz force given by Eq. (2.16). Again, we neglect the small effects due to the vector anisotropic stress of the plasma. This set of vector conservation equations are similar to the one that describes Alfvén waves in Ref. [45]. Equations (4.4), (4.6), (4.8), and (4.9) are not independent. Using the definitions of R , $L_i^{(V)}$, and the fact that $(\rho_\gamma + p_\gamma) \propto 1/a^4$, and solving the Euler equations in the tight-coupling approximation $v_{\gamma i}^{(V)} \simeq v_{bi}^{(V)}$, we obtain the following approximate solution for the vorticity:

$$\Omega_i(\eta, \mathbf{k}) \simeq \frac{k\Pi_i^{(V)}(\mathbf{k})\eta}{(1+R)(\rho_{\gamma 0} + p_{\gamma 0})}. \quad (4.10)$$

Note that the same result can be obtained using Eqs. (4.5) and (4.6). The factor $1+R$ represents reduction in the vorticity due to the Compton drag of baryons. At decoupling, the momentum density ratio between baryons and photons has an approximate value of $R_{\text{dec}} \simeq 3\rho_{b0}/4\rho_{\gamma 0}z_{\text{dec}} \simeq 0.35$, where we have assumed $z_{\text{dec}} = 1100$ and $\Omega_b h^2 = 0.0125$. The vorticity solution of Eq. (4.10) is valid for perturbation wavelengths larger than the comoving Silk scale L_S , where photon viscosity can be neglected compared to the Lorentz force. For $k > k_S$, where $k_S = 2\pi/L_S$, the Euler equation that includes the viscous effect of photons is [56]

$$\left(\frac{4}{3}\rho_\gamma + \rho_b\right)\dot{\Omega}_i + \left(\rho_b\frac{\dot{a}}{a} + \frac{k^2\chi}{a}\right)\Omega_i = \frac{L_i^{(V)}(\mathbf{k})}{a^4}, \quad (4.11)$$

where $\chi = (4/15)\rho_\gamma L_\gamma a$ is the photon shear viscosity coefficient and $L_\gamma = \dot{\tau}^{-1}$ is the photon comoving mean-free path. In this regime, the vorticity can be obtained using the terminal-velocity approximation. Equating the photon viscosity term to the Lorentz force, we obtain [56]

$$\Omega_i(\eta, \mathbf{k}) \simeq \frac{\Pi_i^{(V)}(\mathbf{k})}{(kL_\gamma/5)(\rho_{\gamma 0} + p_{\gamma 0})}, \quad k > k_S. \quad (4.12)$$

The next step is to introduce two-point correlation functions for the vector potential and the vorticity. Defining their two-point correlation functions as in Eq. (2.17) for the vector $\Pi_i^{(V)}$, and taking ensemble averages of Eqs. (4.5), (4.10), and (4.12) the rms isotropic spectra for the vector potential and the vorticity are simply

$$V(\eta, k) = -\frac{16\pi G\Pi^{(V)}(k)\eta}{a^2 k}, \quad (4.13)$$

$$\Omega(\eta, k) \simeq \begin{cases} \frac{k\Pi^{(V)}(k)\eta}{(1+R)(\rho_{\gamma 0} + p_{\gamma 0})}, & k < k_S; \\ \frac{\Pi^{(V)}(k)}{(kL_\gamma/5)(\rho_{\gamma 0} + p_{\gamma 0})}, & k > k_S. \end{cases} \quad (4.14)$$

Vector perturbations induce CMB temperature anisotropies via a Doppler and an integrated Sachs-Wolfe effect [46]:

$$\Theta^{(V)}(\eta_0, \mathbf{k}, \hat{\mathbf{n}}) = -\mathbf{v}^{(V)} \cdot \hat{\mathbf{n}}|_{\eta_{\text{dec}}}^{\eta_0} + \int_{\eta_{\text{dec}}}^{\eta_0} d\eta \dot{\mathbf{V}} \cdot \hat{\mathbf{n}}, \quad (4.15)$$

where η_{dec} represents the conformal time at decoupling. The decaying nature of the vector potential \mathbf{V} implies that most of its contributions toward the integrated Sachs-Wolfe term are around η_{dec} . Neglecting a possible dipole contribution due to $\mathbf{v}^{(V)}$ today, we obtain [46]

$$\Theta^{(V)}(\eta_0, \mathbf{k}, \hat{\mathbf{n}}) \simeq \mathbf{v}^{(V)}(\eta_{\text{dec}}, \mathbf{k}) \cdot \hat{\mathbf{n}} - \mathbf{V}(\eta_{\text{dec}}, \mathbf{k}) \cdot \hat{\mathbf{n}} = \boldsymbol{\Omega}(\eta_{\text{dec}}, \mathbf{k}) \cdot \hat{\mathbf{n}}. \quad (4.16)$$

Vector CMB temperature anisotropies are due to the vorticity at decoupling.

B. Tensor Perturbations

Tensor perturbations to the geometry are described by

$$\delta g_{ij}^{(T)} = 2a^2 h_{ij}, \quad (4.17)$$

where h_{ij} is a symmetric, transverse ($h_{ij}\hat{k}_j = 0$), and traceless ($h_{ii} = 0$) three-tensor. Unlike vector perturbations, tensor perturbations have no gauge freedom.

The tensor Einstein equation that describes the evolution of gravitational waves sourced by a stochastic magnetic field is

$$\ddot{h}_{ij}(\eta, \mathbf{k}) + 2\frac{\dot{a}}{a}\dot{h}_{ij}(\eta, \mathbf{k}) + k^2 h_{ij}(\eta, \mathbf{k}) = 8\pi G\Pi_{ij}^{(T)}(\mathbf{k})/a^2, \quad (4.18)$$

where $\Pi_{ij}^{(T)}(\mathbf{k})$ is given by Eq. (2.19) and as in the case of the vector perturbations, we neglect the tensor anisotropic stress of the plasma, which is in general negligible. Gravitational waves induce CMB temperature anisotropies by causing photons to propagate along perturbed geodesics [58,71]:

$$\Theta^{(T)}(\eta_0, \mathbf{k}, \hat{\mathbf{n}}) \simeq \int_{\eta_{\text{dec}}}^{\eta_0} d\eta \dot{h}_{ij}(\eta, \mathbf{k}) \hat{n}_i \hat{n}_j. \quad (4.19)$$

Our task is, therefore, to obtain the solution for \dot{h}_{ij} . To calculate tensor CMB power spectra, we need to define two-point correlation functions for h_{ij} and \dot{h}_{ij} as in Eq. (2.20) for the tensor $\Pi_{ij}^{(T)}$, with rms isotropic spectra h and \dot{h} respectively. Solutions to the homogeneous equation with $\Pi^{(T)}(k) = 0$ are easily obtained. During the radiation-dominated epoch, $a \propto \eta$ and $h \propto j_0(k\eta)$ or $y_0(k\eta)$, while during the matter-dominated epoch, $a \propto \eta^2$ and $h \propto j_1(k\eta)/k\eta$ or $y_1(k\eta)/k\eta$, where j_l and y_l are the usual spherical Bessel functions. Assuming the primordial stochastic magnetic field is generated at η_{in} , a Green function technique yields the following inhomogeneous solution for the radiation-dominated epoch:

$$h(\eta, k) = \frac{2\pi G\Pi^{(T)}(k)z_{\text{eq}}^2\eta_{\text{eq}}^2}{(3 - 2\sqrt{2})k\eta} \int_{\eta_{\text{in}}}^{\eta} d\eta' \frac{\sin[k(\eta - \eta')]}{\eta'}, \quad \eta < \eta_{\text{eq}}, \quad (4.20)$$

where η_{eq} denotes the conformal time at matter-radiation equality. The magnetic source term on the right hand side of Eq. (4.18) decays more rapidly with η in the matter-dominated epoch than in the radiation-dominated epoch. An approximate solution, therefore, can be obtained by matching the radiation-dominated inhomogeneous solution of Eq. (4.20) to the matter-dominated homogeneous solutions at equality. Retaining the dominant contribution, we obtain [58]

$$\dot{h}(\eta, k) \simeq 4\pi G\eta_0^2 z_{\text{eq}} \ln\left(\frac{z_{\text{in}}}{z_{\text{eq}}}\right) k\Pi^{(T)}(k) \frac{j_2(k\eta)}{k\eta}, \quad \eta > \eta_{\text{eq}}. \quad (4.21)$$

V. TEMPERATURE POWER SPECTRA

We employ the total angular momentum representation introduced by Hu and White [59] to compute the CMB power spectra induced by a primordial stochastic magnetic field. By combining intrinsic angular structure with that of the plane-wave spatial dependence, this representation renders a transparent description of CMB anisotropy formation as each moment corresponds directly to an observable angular sky pattern via its integral solution of the Boltzmann equations. The CMB temperature power spectrum today is given by Eq. (56) of Ref. [59]:

$$C_l^{\Theta\Theta(X)} = \frac{4}{\pi} \int dk k^2 \frac{\Theta_l^{(X)}(\eta_0, k)}{2l+1} \frac{\Theta_l^{(X)*}(\eta_0, k)}{2l+1}, \quad (5.1)$$

where X stands for V or T , and Θ_l 's are the temperature fluctuation $\Delta T/T$ moments. Note that Eq. (5.1) is larger than the corresponding expression in Ref. [59] by a factor of two as we have already taken into account the fact that both vector and tensor perturbations stimulate two modes individually, corresponding to $m = \pm 1, \pm 2$ respectively in the notation of Ref. [59]. Our strategy is to evaluate the Boltzmann temperature integral solutions to obtain the Θ_l 's due to the vector and tensor perturbations. We then substitute them into Eq. (5.1) to yield the corresponding CMB temperature fluctuations spectra. Though the tensor results are already given in Ref. [58], the vector results derived here are new.

A. Vector Temperature Power Spectra

The Boltzmann temperature integral solution for vector perturbations is given by Eqs. (61) and (74) of Ref. [59]:

$$\frac{\Theta_l^{(V)}(\eta_0, k)}{2l+1} = \int_0^{\eta_0} d\eta e^{-\tau} \left\{ (\dot{\tau} v_b^{(V)} + \dot{V}) j_l^{(1V)}[k(\eta_0 - \eta)] + \dot{\tau} P^{(V)} j_l^{(2V)}[k(\eta_0 - \eta)] \right\}, \quad (5.2)$$

where

$$P^{(V)} = \frac{\sqrt{3} k}{9} \frac{k}{\dot{\tau}} v_b^{(V)} \simeq \frac{\sqrt{3} k}{9} \frac{k}{\dot{\tau}} \Omega \quad (5.3)$$

is the vector polarization source that is generated when tight coupling breaks down on small scales, where the photon diffusion length and the perturbation wavelength become comparable. The approximation in Eq. (5.3) is obtained using Eq. (4.3) and noting that Ω dominates V at decoupling [cf. Eqs. (4.13) and (4.14)] for $k \gtrsim 0.006 \text{ Mpc}^{-1}$, resulting in V contributing negligibly compared to Ω upon integrating over k 's to obtain the vector temperature power spectrum in Eq. (5.1). Unlike scalar perturbations, vector perturbations cannot produce compressional modes due to the lack of pressure support. In the usual case of vector perturbations in cosmological fluids without a magnetic field, tight-coupling expansion of photon and baryon Euler equations give $v_b^{(V)} \approx V$, resulting in the vector polarization source being dependent on the vector potential instead (see Eq. (94) of Ref. [59]). A primordial stochastic magnetic field thus enhances vector polarization by sourcing the vorticity. The vector temperature radial functions $j_l^{(1V)}$ and $j_l^{(2V)}$, which describe how distant sources contribute, are given by Eq. (15) of Ref. [59]:

$$\begin{aligned} j_l^{(1V)}(x) &= \sqrt{\frac{l(l+1)}{2}} \frac{j_l(x)}{x}, \\ j_l^{(2V)}(x) &= \sqrt{\frac{3l(l+1)}{2}} \frac{d}{dx} \left(\frac{j_l(x)}{x} \right). \end{aligned} \quad (5.4)$$

The optical depth between η and η_0 is defined as $\tau(\eta) \equiv \int_\eta^{\eta_0} d\eta' \dot{\tau}(\eta')$, thus $d\tau/d\eta = -\dot{\tau}$. Integrating Eq. (5.2) by parts using $de^{-\tau}/d\eta = \dot{\tau}e^{-\tau}$ and $j_l^{(2V)}(x) = \sqrt{3}(j_l^{(1V)}(x))'$ and Eqs. (4.3) and (5.3), we obtain

$$\frac{\Theta_l^{(V)}(\eta_0, k)}{2l+1} = \int_0^{\eta_0} d\eta \dot{\tau} e^{-\tau} \left\{ \Omega j_l^{(1V)}[k(\eta_0 - \eta)] + \frac{\sqrt{3} k}{9} \frac{k}{\dot{\tau}} (\Omega + 3V) j_l^{(2V)}[k(\eta_0 - \eta)] \right\}. \quad (5.5)$$

For the usual vector perturbations without a magnetic field, the term proportional to $j_l^{(1V)}$ is strongly suppressed since $v_b^{(V)} \approx V$ at decoupling [59] and hence $\Omega \simeq 0$ as mentioned above. Here we have a primordial stochastic magnetic field sourcing Ω ; the term proportional to $j_l^{(2V)}$ is then suppressed relative to the term proportional to $j_l^{(1V)}$ due to the factor $k/\dot{\tau}$. Moreover, $j_l^{(2V)}$ has less angular power compared to $j_l^{(1V)}$ (see Fig. 3 of Ref. [59]). Thus to simplify the calculation, we consider only the term proportional to $j_l^{(1V)}$ in computing the vector temperature integral solution. Including the small corrections due to the angular dependence of polarization coming from the term proportional to $P^{(V)} j_l^{(2V)}$ and also the vector potential will yield an additional contribution of at most a few percent toward our final estimate of the vector temperature power spectra. The combination $\dot{\tau}e^{-\tau}$ is the conformal visibility function, which represents the probability that a photon last scattered within $d\eta$ of η and hence is sharply peaked at the decoupling period. For $l \leq 500$, we can approximate the vector temperature integral solution reasonably well as

$$\frac{\Theta_l^{(V)}(\eta_0, k)}{2l+1} \simeq \sqrt{\frac{l(l+1)}{2}} \Omega(\eta_{\text{dec}}, k) \frac{j_l(k\eta_0)}{k\eta_0}, \quad (5.6)$$

using Eq. (5.4) and the fact that $\eta_0 \gg \eta_{\text{dec}}$. The vector CMB temperature anisotropies are due to the vorticity at decoupling, as also illustrated by Eq. (4.16). Substituting Eq. (5.6) into the CMB temperature power spectrum expression of Eq. (5.1) and using Eqs. (4.14) and (2.18), we obtain

$$\begin{aligned} C_l^{\Theta\Theta(V)} &= \frac{(2\pi)^{2n+11}}{4} l(l+1) \frac{v_{A\lambda}^4}{\Gamma^2\left(\frac{n+3}{2}\right) (2n+3)} \frac{(k_D \eta_0)^{2n+3}}{(k_\lambda \eta_0)^{2n+6}} \left[\frac{\eta_{\text{dec}}^2}{(1+R_{\text{dec}})^2} \int_0^{k_S} dk k + \frac{25}{L_{\gamma \text{dec}}^2} \int_{k_S}^{k_D} \frac{dk}{k^3} \right] \\ &\times \left[1 + \frac{n}{n+3} \left(\frac{k}{k_D} \right)^{2n+3} \right] J_{l+1/2}^2(k\eta_0), \end{aligned} \quad (5.7)$$

where we have defined the Alfvén velocity as $v_{A\lambda} = B_\lambda/[4\pi(\rho_{\gamma 0} + p_{\gamma 0})]^{1/2} \simeq 3.8 \times 10^{-4}(B_\lambda/10^{-9} \text{ G})$. Note that $(2\pi)^{2n+10}v_{A\lambda}^4/[\Gamma^2(\frac{n+3}{2})k_\lambda^{2n+6}] \propto A^2$, where A is the normalization of the magnetic power spectrum in Eq. (2.5).

Depending on whether $n > -3/2$ or $-3 < n < -3/2$, we retain only the corresponding dominant term of the vector isotropic spectrum in Eq. (5.7). First consider the case $n > -3/2$, where the vorticity source becomes approximately white noise (independent of k) and that $|\Pi^{(V)}(k)|^2$ is dependent on k_D . To obtain an analytic estimate of the integral $\int_0^{k_S} dk k J_{l+1/2}^2(k\eta_0)$, consider the more general integral $\int_0^{x_S} dx x^p J_l^2(x)$ for some $p \geq 0$. Since $J_l^2(x)$ only begins to contribute to the integral significantly when $x \gtrsim l$, in this limit, we employ in the integral the $J_l(x)$ asymptotic expansion for large argument [72]: $J_l(x) \sim \sqrt{2/(\pi x)} \cos[x - (2l+1)\pi/4]$. Approximating the oscillations by a factor of one half then gives

$$\int_0^{x_S} dx x^p J_l^2(x) \simeq \int_l^{x_S} dx x^p J_l^2(x) \simeq \begin{cases} \frac{x_S^{p-1}}{p\pi}, & p > 0; \\ \frac{1}{\pi} \ln\left(\frac{x_S}{l}\right), & p = 0. \end{cases} \quad (5.8)$$

The approximation tends to underestimate; it is good to a few percent for $p > 1$ and is within 30% for $0 \leq p \leq 1$. The integral $\int_0^{k_S} dk k J_{l+1/2}^2(k\eta_0)$ corresponds to the case $p = 1$; the remaining integral on the rhs of Eq. (5.7) $\int_{k_S}^{k_D} dk k^{-3} J_{l+1/2}^2(k\eta_0)$ can be well-approximated by $(k_S^{-3} - k_D^{-3})/(3\pi\eta_0)$, which is good to within 20%. As in Eq. (5.8), this approximation is obtained via employing the Bessel function asymptotic expansion for large argument, which is justified since $k\eta_0 > l$ for $k_S \leq k \leq k_D$ and $l \leq 500$. Keeping only the highest-order term in l , we obtain the vector CMB temperature power spectrum for $n > -3/2$:

$$l^2 C_l^{\Theta\Theta(V)} = \frac{(2\pi)^{2n+10}}{2} \frac{v_{A\lambda}^4 l^4}{\Gamma^2\left(\frac{n+3}{2}\right) (2n+3)} \frac{(k_D\eta_0)^{2n+3}}{(k_\lambda\eta_0)^{2n+6}} \left\{ \left(\frac{\eta_{\text{dec}}/\eta_0}{1+R_{\text{dec}}} \right)^2 (k_S\eta_0 - l) \right. \\ \left. + \frac{25}{3} \left(\frac{\eta_0}{L_{\gamma \text{ dec}}} \right)^2 \left[\frac{1}{(k_S\eta_0)^3} - \frac{1}{(k_D\eta_0)^3} \right] \right\}, \quad n > -3/2. \quad (5.9)$$

The dominant contribution comes from the term proportional to $(k_S\eta_0 - l)$, which arises from the non-damped vorticity for $k < k_S$. The remaining term arising from the damped vorticity for $k_S < k < k_D$ gives a negligible contribution of $< 1\%$. A numerical evaluation of Eq. (5.7) shows that its second integral on the rhs, which arises from the damped vorticity, always contribute negligibly ($< 1\%$) compared to its first integral for $l \leq 500$ and all cases of n . Therefore, we will neglect the damped vorticity contribution when evaluating the remaining vector CMB temperature power spectra.

For $-3 < n < -3/2$, the needed integral is $\int_0^{k_S} dk k^{2n+4} J_{l+1/2}^2(k\eta_0)$. We must consider three cases depending on whether the exponent $2n+4$ is greater than, equal to, or less than zero. For $-2 < n < -3/2$, using Eq. (5.8) for $p = 2n+4$, we obtain

$$l^2 C_l^{\Theta\Theta(V)} = \frac{(2\pi)^{2n+10}}{4} \left(\frac{\eta_{\text{dec}}/\eta_0}{1+R_{\text{dec}}} \right)^2 \frac{v_{A\lambda}^4 n l^4}{\Gamma^2\left(\frac{n+3}{2}\right) (2n+3)(n+2)(n+3)(k_\lambda\eta_0)^{2n+6}} [(k_S\eta_0)^{2n+4} - l^{2n+4}], \\ -2 < n < -3/2. \quad (5.10)$$

For $n = -2$, again using Eq. (5.8) for $p = 0$, we obtain

$$l^2 C_l^{\Theta\Theta(V)} = 2(2\pi)^5 \left(\frac{\eta_{\text{dec}}/\eta_0}{1+R_{\text{dec}}} \right)^2 \frac{v_{A\lambda}^4 l^4}{(k_\lambda\eta_0)^2} \ln\left(\frac{k_S\eta_0}{l}\right), \quad n = -2. \quad (5.11)$$

For $-3 < n < -2$, numerical evaluation shows that for $-2.3 \lesssim n < -2$, the integral $\int_0^{k_S} dk k^{2n+4} J_{l+1/2}^2(k\eta_0)$ can be well-approximated by $[(k_S\eta_0)^{2n+4} - l^{2n+4}]/[2\pi(n+2)\eta_0^{2n+5}]$, which underestimates by at most 30–40%. The resulting temperature power spectrum is then formally identical to that of the case $-2 < n < -3/2$:

$$l^2 C_l^{\Theta\Theta(V)} = \frac{(2\pi)^{2n+10}}{4} \left(\frac{\eta_{\text{dec}}/\eta_0}{1+R_{\text{dec}}} \right)^2 \frac{v_{A\lambda}^4 n l^4}{\Gamma^2\left(\frac{n+3}{2}\right) (2n+3)(n+2)(n+3)(k_\lambda\eta_0)^{2n+6}} [(k_S\eta_0)^{2n+4} - l^{2n+4}], \\ -2.3 \lesssim n < -2. \quad (5.12)$$

For $-3 < n \lesssim -2.3$, the dominant contribution to the integral $\int_0^{k_S} dk k^{2n+4} J_{l+1/2}^2(k\eta_0)$ is coming from long wavelengths $k \rightarrow 0$, we therefore approximate by integrating over k to infinity. The resulting integral can be evaluated analytically by using 6.574.2 of Ref. [73],

$$\int_0^\infty dk J_p(ak)J_q(ak)k^{-b} = \frac{a^{b-1}\Gamma(b)\Gamma\left(\frac{p+q-b+1}{2}\right)}{2^b\Gamma\left(\frac{-p+q+b+1}{2}\right)\Gamma\left(\frac{p+q+b+1}{2}\right)\Gamma\left(\frac{p-q+b+1}{2}\right)}, \quad \text{Re}(p+q+1) > \text{Re} b > 0, a > 0; \quad (5.13)$$

and 8.335.1 of Ref. [73],

$$\Gamma(2x) = \frac{2^{2x-1}}{\sqrt{\pi}}\Gamma(x)\Gamma\left(x + \frac{1}{2}\right). \quad (5.14)$$

Keeping only the highest-order term in l , we finally obtain

$$l^2 C_l^{\Theta\Theta(V)} = \frac{(2\pi)^{2n+10}}{2^{2n+7}} \left(\frac{\eta_{\text{dec}}/\eta_0}{1 + R_{\text{dec}}}\right)^2 \frac{\Gamma^2(-n-2)}{\Gamma(-2n-4)\Gamma^2\left(\frac{n+3}{2}\right)} \frac{v_{A\lambda}^4 n l^{2n+8}}{(2n+3)(n+3)(k_\lambda \eta_0)^{2n+6}}, \quad -3 < n \lesssim -2.3. \quad (5.15)$$

Our approximation overestimates, as expected, and the accuracy improves as n decreases since more contribution arises from small k and hence the result will be less sensitive to the upper limit of the integral, which we have approximated to be infinity. It is good to within 30% for $-2.5 < n \lesssim -2.3$ and a few percent for $-3 < n < -2.5$. The temperature power spectrum of each case above has the same l and k_D (with $k_\lambda, k_S \rightarrow k_D$) dependence as the corresponding spectrum induced by a primordial homogeneous magnetic field [46] (the correspondence between the spectral index of Ref. [46] and ours is $n \rightarrow 2n+3$). For the sake of completeness, we note that the vector potential contribution arising from the $j_i^{(2V)}$ term in Eq. (5.5) will induce temperature power spectra $l^2 C_l^{\Theta\Theta(V)} \propto l^3$ for $n > -3/2$ and $l^2 C_l^{\Theta\Theta(V)} \propto l^{2n+6}$ for $-3 < n < -3/2$.

We now consider the case $n = -3/2$ and show that this apparent singularity is removable by considering both terms of the vector isotropic spectrum in Eq. (2.18). In the limit $n = -3/2 + \varepsilon$, we have

$$|\Pi^{(V)}(k)|^2 \simeq \frac{(2\pi)^6}{16} \frac{B_\lambda^4}{\Gamma^2(3/4)k_\lambda^3} \frac{1}{2\varepsilon} \left[1 - \left(1 - \frac{2\varepsilon}{3}\right) \left(1 + \frac{2\varepsilon}{3}\right)^{-1} \left(\frac{k}{k_D}\right)^{2\varepsilon} \right]. \quad (5.16)$$

Upon expanding the expression within the square bracket to $\mathcal{O}(\varepsilon)$ and using the small- x expansion to the first order, i.e. $\ln(1+x) \sim x$ for $x \equiv (k - k_D)/k_D$, we obtain

$$|\Pi^{(V)}(k)|^2 \simeq \frac{(2\pi)^6}{16} \frac{B_\lambda^4}{\Gamma^2(3/4)k_\lambda^3} \left(\frac{5}{3} - \frac{k}{k_D}\right), \quad n \approx -3/2. \quad (5.17)$$

The same result can be obtained via direct substitution of $n = -3/2$ in Eqs. (A9) to (A11). Using Eqs. (5.17) and (5.8) for $p = 1$ and 2, a similar calculation as in Eq. (5.9) gives

$$l^2 C_l^{\Theta\Theta(V)} = \frac{(2\pi)^7}{4} \left(\frac{\eta_{\text{dec}}/\eta_0}{1 + R_{\text{dec}}}\right)^2 \frac{v_{A\lambda}^4 l^4}{\Gamma^2(3/4)(k_\lambda \eta_0)^3} \left[\frac{10}{3}(k_S \eta_0 - l) - \frac{(k_S \eta_0)^2 - l^2}{k_D \eta_0} \right], \quad n \approx -3/2, \quad (5.18)$$

thus showing that the singularity at $n = -3/2$ is indeed removable. For the rest of the paper, we will not produce explicit power spectrum expressions for the case $n = -3/2$. Readers who are interested can easily derive the corresponding results via a straightforward extension of the calculation outlined above.

B. Tensor Temperature Power Spectra

The Boltzmann temperature integral solution for tensor perturbations is given by Eqs. (61) and (74) of Ref. [59]:

$$\frac{\Theta_l^{(T)}(\eta_0, k)}{2l+1} = \int_0^{\eta_0} d\eta e^{-\tau} [\dot{\tau} P^{(T)} - \dot{h}] j_l^{(2T)}[k(\eta_0 - \eta)], \quad (5.19)$$

where

$$P^{(T)} = -\frac{1}{3} \frac{\dot{h}}{\dot{\tau}} \quad (5.20)$$

is the tensor polarization source and $j_l^{(2T)}$ is the tensor temperature radial function given by Eq. (15) of Ref. [59]:

$$j_l^{(2T)}(x) = \sqrt{\frac{3(l+2)!}{8(l-2)!}} \frac{j_l(x)}{x^2}. \quad (5.21)$$

Using Eq. (4.21) and defining $x \equiv k\eta$ and $x_0 \equiv k\eta_0$, we approximate the tensor temperature integral solution as (see also Eq. (18) of Ref. [58])

$$\frac{\Theta_l^{(T)}(\eta_0, k)}{2l+1} \simeq -2\pi \sqrt{\frac{8(l+2)!}{3(l-2)!}} \left[G\eta_0^2 z_{\text{eq}} \ln\left(\frac{z_{\text{in}}}{z_{\text{eq}}}\right) \right] \Pi^{(T)}(k) \int_0^{x_0} dx \frac{j_2(x)}{x} \frac{j_l(x_0-x)}{(x_0-x)^2}. \quad (5.22)$$

The integral above can be numerically approximated as in Eq. (19) of Ref. [58],

$$\begin{aligned} \int_0^{x_0} dx \frac{j_2(x)}{x} \frac{j_l(x_0-x)}{(x_0-x)^2} &= \frac{\pi}{2} \int_0^{x_0} dx \frac{J_{5/2}(x)}{x^{3/2}} \frac{J_{l+1/2}(x_0-x)}{(x_0-x)^{5/2}} \\ &\simeq \frac{7\pi}{20} \sqrt{l} \int_0^{x_0} dx \frac{J_{5/2}(x)}{x} \frac{J_{l+1/2}(x_0-x)}{(x_0-x)^3} \\ &\simeq \frac{7\pi}{50} \sqrt{\frac{3l}{2}} \frac{J_{l+3}(x_0)}{x_0^3}, \end{aligned} \quad (5.23)$$

where in going from the second to the third line, we have inserted a factor of $\sqrt{3/2}$ for better numerical agreement and used 6.581.2 of Ref. [73]:

$$\int_0^a dx x^{b-1} (a-x)^{-1} J_p(x) J_q(a-x) = \frac{2^b}{aq} \sum_{m=0}^{\infty} \frac{(-1)^m \Gamma(b+p+m) \Gamma(b+m)}{m! \Gamma(b) \Gamma(p+m+1)} (b+p+q+2m) J_{b+p+q+2m}(a), \quad (5.24)$$

$\text{Re}(b+p) > 0, \text{Re} q > 0.$

Numerical evaluation shows that the approximation in the second line of Eq. (5.23) is good to 10% for $l \lesssim 500$. Substituting Eq. (5.23) into Eq. (5.22) yields

$$\frac{\Theta_l^{(T)}(\eta_0, k)}{2l+1} \simeq -\frac{7}{50} (2\pi)^2 \sqrt{\frac{l(l+2)!}{(l-2)!}} \left[G\eta_0^2 z_{\text{eq}} \ln\left(\frac{z_{\text{in}}}{z_{\text{eq}}}\right) \right] \Pi^{(T)}(k) \frac{J_{l+3}(k\eta_0)}{(k\eta_0)^3}. \quad (5.25)$$

Using Eqs. (2.22), (5.1), and (5.25), we obtain

$$\begin{aligned} C_l^{\Theta\Theta(T)} &= \frac{49}{10000} (2\pi)^{2n+12} l^2 (l-1)(l+1)(l+2) \left[G\eta_0^2 z_{\text{eq}} \ln\left(\frac{z_{\text{in}}}{z_{\text{eq}}}\right) \right]^2 \frac{B_\lambda^4}{\Gamma^2\left(\frac{n+3}{2}\right) (2n+3)\eta_0^3} \frac{(k_D\eta_0)^{2n+3}}{(k_\lambda\eta_0)^{2n+6}} \\ &\times \int_0^{k_D} dk k^{-4} \left[1 + \frac{n}{n+3} \left(\frac{k}{k_D}\right)^{2n+3} \right] J_{l+3}^2(k\eta_0). \end{aligned} \quad (5.26)$$

Note that $(2\pi)^{2n+10} B_\lambda^4 / [\Gamma^2(\frac{n+3}{2}) k_\lambda^{2n+6}] \propto A^2$, where A is the normalization of the magnetic power spectrum in Eq. (2.5).

For $n > -3/2$, the gravitational wave source is k_D -dependent, and the resulting temperature fluctuation spectrum possesses the well-known behavior $l^2 C_l \propto l^3$. The integral $\int_0^{k_D} dk k^{-4} J_{l+3}^2(k\eta_0)$ can be evaluated using Eq. (5.13); retaining only the highest-order term in l , we obtain

$$l^2 C_l^{\Theta\Theta(T)} = \frac{49}{7500} (2\pi)^{2n+11} \left[G\eta_0^2 z_{\text{eq}} \ln\left(\frac{z_{\text{in}}}{z_{\text{eq}}}\right) \right]^2 \frac{B_\lambda^4 l^3}{\Gamma^2\left(\frac{n+3}{2}\right) (2n+3)} \frac{(k_D\eta_0)^{2n+3}}{(k_\lambda\eta_0)^{2n+6}}, \quad n > -3/2. \quad (5.27)$$

For $-3 < n < -3/2$, a similar calculation gives

$$\begin{aligned} l^2 C_l^{\Theta\Theta(T)} &= 2^{2n-5} \frac{49}{625} (2\pi)^{2n+12} \left[G\eta_0^2 z_{\text{eq}} \ln\left(\frac{z_{\text{in}}}{z_{\text{eq}}}\right) \right]^2 \frac{\Gamma(1-2n)}{\Gamma^2(1-n) \Gamma^2\left(\frac{n+3}{2}\right)} \frac{B_\lambda^4 n}{(2n+3)(n+3)} \left(\frac{l}{k_\lambda\eta_0}\right)^{2n+6}, \\ &-3 < n < -3/2. \end{aligned} \quad (5.28)$$

Equivalent tensor perturbation results are given in Eqs. (20) to (22) of Ref. [58].

VI. POLARIZATION POWER SPECTRA

Polarization of the CMB comes in two flavors: E-type and B-type with electric $(-1)^l$ and magnetic $(-1)^{l+1}$ parities respectively [74,75]. Physically, they represent polarization patterns rotated by $\pi/4$ due to the interchanging of Q and U Stokes parameters. Vector and tensor perturbations induce both types of polarizations. Scalar perturbations, however, cannot generate B-type polarization due to azimuthal symmetry. A detection of the B-type polarization from future high sensitivity CMB polarization measurements therefore would provide compelling evidence for vector and/or tensor contributions. Similar to the CMB temperature power spectrum of Eq. (5.1), the E-type and B-type polarization power spectra are respectively

$$C_l^{EE(X)} = \frac{4}{\pi} \int dk k^2 \frac{E_l^{(X)}(\eta_0, k)}{2l+1} \frac{E_l^{(X)*}(\eta_0, k)}{2l+1}, \quad (6.1)$$

$$C_l^{BB(X)} = \frac{4}{\pi} \int dk k^2 \frac{B_l^{(X)}(\eta_0, k)}{2l+1} \frac{B_l^{(X)*}(\eta_0, k)}{2l+1}, \quad (6.2)$$

where X stands for V or T . The correspondence between notations of Ref. [59] and ours for polarization moments are $E_l^{(\pm 1)} \rightarrow E_l^{(V)}$ and $B_l^{(\pm 1)} \rightarrow \pm B_l^{(V)}$, and similarly for the tensor perturbations.

A. Vector Polarization Power Spectra

1. E-type Polarization

The E-type polarization integral solution for vector perturbations is [59]

$$\frac{E_l^{(V)}(\eta_0, k)}{2l+1} = -\sqrt{6} \int_0^{\eta_0} d\eta \dot{\tau} e^{-\tau} P^{(V)} \epsilon_l^{(V)}[k(\eta_0 - \eta)], \quad (6.3)$$

where

$$\epsilon_l^{(V)}(x) = \frac{1}{2} \sqrt{(l-1)(l+2)} \left[\frac{j_l(x)}{x^2} + \frac{j_l'(x)}{x} \right] \quad (6.4)$$

is the vector E-type polarization radial function given by Eq. (17) of Ref. [59]. Using Eq. (5.3) for $P^{(V)}$ and the spherical Bessel function recurrence relation [72]

$$\frac{l}{x} j_l(x) - j_l'(x) = j_{l+1}(x), \quad (6.5)$$

we approximate the vector E-type polarization integral solution as in Eq. (5.6):

$$\frac{E_l^{(V)}(\eta_0, k)}{2l+1} \simeq -\sqrt{\frac{(l-1)(l+2)}{18}} k L_{\gamma \text{dec}} \Omega(\eta_{\text{dec}}, k) \left[(l+1) \frac{j_l(k\eta_0)}{(k\eta_0)^2} - \frac{j_{l+1}(k\eta_0)}{k\eta_0} \right], \quad (6.6)$$

where $L_{\gamma \text{dec}} = \dot{\tau}_{\text{dec}}^{-1} \simeq 3.39 \text{ Mpc}$ is the photon comoving mean-free path at decoupling, assuming $T_{\text{dec}} = 0.25 \text{ eV}$ and $\Omega_b h^2 = 0.0125$. For the tight-coupling approximation to be valid, we require $k L_{\gamma \text{dec}} < 1$. Substituting Eq. (6.6) into (6.1) and using Eqs. (4.14) and (2.18), we obtain

$$C_l^{EE(V)} = \frac{(2\pi)^{2n+11}}{36} (l-1)(l+2) \left(\frac{\eta_{\text{dec}} \eta_0}{1+R_{\text{dec}}} \right)^2 \frac{v_{A\lambda}^4}{\Gamma^2 \left(\frac{n+3}{2} \right) (2n+3)} \frac{(k_D \eta_0)^{2n+3}}{(k_\lambda \eta_0)^{2n+6}} \\ \times L_{\gamma \text{dec}}^2 \int_0^{k_S} dk k^5 \left[1 + \frac{n}{n+3} \left(\frac{k}{k_D} \right)^{2n+3} \right] \left[(l+1) \frac{J_{l+1/2}(k\eta_0)}{(k\eta_0)^2} - \frac{J_{l+3/2}(k\eta_0)}{k\eta_0} \right]^2. \quad (6.7)$$

As in the computation of the vector temperature power spectra in Sec. V A, we have neglected the damped vorticity term, which again contributes negligibly ($< 3\%$) for $l \leq 500$ and all cases of n . Note that $(2\pi)^{2n+10} v_{A\lambda}^4 / [\Gamma^2 \left(\frac{n+3}{2} \right) k_\lambda^{2n+6}] \propto A^2$, where A is the normalization of the magnetic power spectrum in Eq. (2.5).

Again, depending on whether $n > -3/2$ or $-3 < n < -3/2$, we retain only the corresponding dominant term of the vector isotropic spectrum in Eq. (6.7). A further simplification occurs by noting that although the cross term proportional to $J_{l+1/2}(k\eta_0)J_{l+3/2}(k\eta_0)$ is difficult to evaluate analytically, a numerical evaluation shows that its value is approximately minus twice that of the term proportional to $J_{l+1/2}^2(k\eta_0)$ for all cases of n . First consider the case $n > -3/2$, where the vorticity source becomes approximately white noise and is k_D -dependent. The relevant integrals are

$$(l+1)^2 \int_0^{x_S} dx x J_{l+1/2}^2(x) \quad \text{and} \quad \int_0^{x_S} dx x^3 J_{l+3/2}^2(x), \quad (6.8)$$

where we have defined $x \equiv k\eta_0$ and $x_S \equiv k_S\eta_0$. Using Eq. (5.8) for $p = 1$ and 3 respectively for these two integrals, we obtain

$$l^2 C_l^{EE(V)} = \frac{(2\pi)^{2n+10}}{18} \left(\frac{\eta_{\text{dec}}/\eta_0}{1+R_{\text{dec}}} \right)^2 \left(\frac{L_{\gamma \text{ dec}}}{\eta_0} \right)^2 \frac{v_{A\lambda}^4 l^4}{\Gamma^2\left(\frac{n+3}{2}\right) (2n+3)} \frac{(k_D\eta_0)^{2n+3}}{(k_\lambda\eta_0)^{2n+6}} \left[\frac{(k_S\eta_0)^3 - l^3}{3} - l^2(k_S\eta_0 - l) \right], \quad n > -3/2. \quad (6.9)$$

Comparing to the numerical evaluation of Eq. (6.7) shows that our approximation is good to a few percent.

For $-3 < n < -3/2$, we need to evaluate

$$(l+1)^2 \int_0^{x_S} dx x^{2n+4} J_{l+1/2}^2(x) \quad \text{and} \quad \int_0^{x_S} dx x^{2n+6} J_{l+3/2}^2(x). \quad (6.10)$$

Since the exponent within the first integral $2n+4$ changes sign whereas the exponent within the second integral $2n+6$ remains positive throughout $-3 < n < -3/2$, as in the vector temperature power spectra calculation, we consider cases depending on whether $2n+4$ is greater than, equal to, or less than zero in this regime. For $-2 < n < -3/2$, the two integrals of Eq. (6.10) can be approximated using Eq. (5.8) for $p = 2n+4$ and $2n+6$ respectively, hence

$$l^2 C_l^{EE(V)} = \frac{(2\pi)^{2n+10}}{36} \left(\frac{\eta_{\text{dec}}/\eta_0}{1+R_{\text{dec}}} \right)^2 \left(\frac{L_{\gamma \text{ dec}}}{\eta_0} \right)^2 \frac{v_{A\lambda}^4 n l^4}{\Gamma^2\left(\frac{n+3}{2}\right) (2n+3)(n+3)(k_\lambda\eta_0)^{2n+6}} \times \left[\frac{(k_S\eta_0)^{2n+6} - l^{2n+6}}{n+3} - l^2 \frac{(k_S\eta_0)^{2n+4} - l^{2n+4}}{n+2} \right], \quad -2 < n < -3/2. \quad (6.11)$$

Here our approximation is good to within 10%. For $n = -2$, using Eq. (5.8) for $p = 0$ and 2 respectively for the two integrals of Eq. (6.10), we obtain

$$l^2 C_l^{EE(V)} = \frac{(2\pi)^5}{9} \left(\frac{\eta_{\text{dec}}/\eta_0}{1+R_{\text{dec}}} \right)^2 \left(\frac{L_{\gamma \text{ dec}}}{\eta_0} \right)^2 \frac{v_{A\lambda}^4 l^4}{(k_\lambda\eta_0)^2} \left\{ (k_S\eta_0)^2 - l^2 \left[2 \ln \left(\frac{k_S\eta_0}{l} \right) + 1 \right] \right\}, \quad n = -2. \quad (6.12)$$

Comparing to the numerical evaluation of Eq. (6.7), the approximation here is good to within 10% in general. For $-3 < n < -2$, as discussed in Sec. V A, a numerical evaluation shows that the first integral of Eq. (6.10) can be well-approximated by $l^2[(k_S\eta_0)^{2n+4} - l^{2n+4}]/(2n+4)\pi$ for $-2.3 \lesssim n < -2$ [cf. Eq. (5.12)] whereas for $-3 < n \lesssim -2.3$, it can be approximated using Eq. (5.13) since the dominant contribution to the integral arises from long wavelengths $k \rightarrow 0$ [cf. Eq. (5.15)]. The approximation of the second integral of Eq. (6.10) using Eq. (5.8) tends to underestimate. This, however, can be compensated via approximating the first integral of Eq. (6.10) by $l^2[(k_S\eta_0)^{2n+4} - l^{2n+4}]/(2n+4)\pi$ throughout the regime $-3 < n < -2$. The resulting vector E-type polarization power spectrum is then formally identical to that of the case $-2 < n < -3/2$, with accuracy good to within 15% in general. Hence

$$l^2 C_l^{EE(V)} = \frac{(2\pi)^{2n+10}}{36} \left(\frac{\eta_{\text{dec}}/\eta_0}{1+R_{\text{dec}}} \right)^2 \left(\frac{L_{\gamma \text{ dec}}}{\eta_0} \right)^2 \frac{v_{A\lambda}^4 n l^4}{\Gamma^2\left(\frac{n+3}{2}\right) (2n+3)(n+3)(k_\lambda\eta_0)^{2n+6}} \times \left[\frac{(k_S\eta_0)^{2n+6} - l^{2n+6}}{n+3} - l^2 \frac{(k_S\eta_0)^{2n+4} - l^{2n+4}}{n+2} \right], \quad -3 < n < -2. \quad (6.13)$$

2. B-type Polarization

The B-type polarization integral solution for vector perturbations is [59]

$$\frac{B_l^{(V)}(\eta_0, k)}{2l+1} = -\sqrt{6} \int_0^{\eta_0} d\eta \dot{\tau} e^{-\tau} P^{(V)} \beta_l^{(V)}[k(\eta_0 - \eta)], \quad (6.14)$$

where

$$\beta_l^{(V)}(x) = \frac{1}{2} \sqrt{(l-1)(l+2)} \frac{j_l(x)}{x} \quad (6.15)$$

is the vector B-type polarization radial function. Using the same approximation in Eq. (6.14) as in Eq. (5.6), we obtain

$$\frac{B_l^{(V)}(\eta_0, k)}{2l+1} \simeq -\sqrt{\frac{(l-1)(l+2)}{18}} k L_{\gamma \text{ dec}} \Omega(\eta_{\text{dec}}, k) \frac{j_l(k\eta_0)}{k\eta_0}, \quad (6.16)$$

which upon substituting into Eq. (6.2) and using Eqs. (4.14) and (2.18), yields

$$\begin{aligned} C_l^{BB(V)} &= \frac{(2\pi)^{2n+11}}{36} (l-1)(l+2) \left(\frac{\eta_{\text{dec}} \eta_0}{1+R_{\text{dec}}} \right)^2 \frac{v_{A\lambda}^4}{\Gamma^2\left(\frac{n+3}{2}\right) (2n+3)} \frac{(k_D \eta_0)^{2n+3}}{(k_\lambda \eta_0)^{2n+6}} \\ &\quad \times L_{\gamma \text{ dec}}^2 \int_0^{k_S} dk k^5 \left[1 + \frac{n}{n+3} \left(\frac{k}{k_D} \right)^{2n+3} \right] \frac{J_{l+1/2}^2(k\eta_0)}{(k\eta_0)^2}, \end{aligned} \quad (6.17)$$

where again we have neglected the contribution coming from the damped vorticity term, which is negligible ($< 4\%$) for $l \leq 500$ and all cases of n . Note that $(2\pi)^{2n+10} v_{A\lambda}^4 / [\Gamma^2\left(\frac{n+3}{2}\right) k_\lambda^{2n+6}] \propto A^2$, where A is the normalization of the magnetic power spectrum in Eq. (2.5). Except for the order of the Bessel function, Eq. (6.17) is identical to the term proportional to $J_{l+3/2}^2(k\eta_0)$ in the vector E-type polarization power spectrum expression of Eq. (6.7). For $n > -3/2$, using Eq. (5.8) for $p = 3$, we obtain [cf. Eq. (6.9)]

$$l^2 C_l^{BB(V)} = \frac{(2\pi)^{2n+10}}{54} \left(\frac{\eta_{\text{dec}}/\eta_0}{1+R_{\text{dec}}} \right)^2 \left(\frac{L_{\gamma \text{ dec}}}{\eta_0} \right)^2 \frac{v_{A\lambda}^4 l^4}{\Gamma^2\left(\frac{n+3}{2}\right) (2n+3)} \frac{(k_D \eta_0)^{2n+3}}{(k_\lambda \eta_0)^{2n+6}} [(k_S \eta_0)^3 - l^3], \quad n > -3/2. \quad (6.18)$$

For $-3 < n < -3/2$, the exponent within the integral $2n+6$ remains positive throughout; thus using Eq. (5.8) for $p = 2n+6$, we obtain [cf. Eq. (6.11)]

$$\begin{aligned} l^2 C_l^{BB(V)} &= \frac{(2\pi)^{2n+10}}{36} \left(\frac{\eta_{\text{dec}}/\eta_0}{1+R_{\text{dec}}} \right)^2 \left(\frac{L_{\gamma \text{ dec}}}{\eta_0} \right)^2 \frac{v_{A\lambda}^4 n l^4}{\Gamma^2\left(\frac{n+3}{2}\right) (2n+3)(n+3)^2 (k_\lambda \eta_0)^{2n+6}} [(k_S \eta_0)^{2n+6} - l^{2n+6}], \\ &\quad -3 < n < -3/2. \end{aligned} \quad (6.19)$$

Our accuracy here is good to the quality of the analytic approximation in Eq. (5.8) and is always within 20%.

B. Tensor Polarization Power Spectra

1. E-type Polarization

The E-type polarization integral solution for tensor perturbations is [59]

$$\frac{E_l^{(T)}(\eta_0, k)}{2l+1} = -\sqrt{6} \int_0^{\eta_0} d\eta \dot{\tau} e^{-\tau} P^{(T)} \epsilon_l^{(T)}[k(\eta_0 - \eta)], \quad (6.20)$$

where $P^{(T)}$ is given by Eq. (5.20), and

$$\epsilon_l^{(T)}(x) = \frac{1}{4} \left[-j_l(x) + j_l''(x) + 2 \frac{j_l(x)}{x^2} + 4 \frac{j_l'(x)}{x} \right] \quad (6.21)$$

is the tensor E-type polarization radial function. Using Eqs. (4.21) and (6.5) and the spherical Bessel function recurrence relation [72]

$$\frac{l+1}{x} j_l(x) + j_l'(x) = j_{l-1}(x), \quad (6.22)$$

and defining $x \equiv k\eta$ and $x_0 \equiv k\eta_0$, we approximate the tensor E-type polarization integral solution as

$$\begin{aligned} \frac{E_l^{(T)}(\eta_0, k)}{2l+1} &\simeq \frac{2\pi}{\sqrt{6}} \left[G\eta_0^2 z_{\text{eq}} \ln \left(\frac{z_{\text{in}}}{z_{\text{eq}}} \right) \right] \Pi^{(T)}(k) \\ &\times \int_0^{x_0} dx \frac{j_2(x)}{x} \left\{ \left[-2 + \frac{(l+1)(l+2)}{(x_0-x)^2} \right] j_l(x_0-x) - \frac{2}{x_0-x} j_{l+1}(x_0-x) \right\}. \end{aligned} \quad (6.23)$$

A similar manipulation as in Eq. (5.23) gives

$$\frac{E_l^{(T)}(\eta_0, k)}{2l+1} \simeq -\frac{7}{100} (2\pi)^2 \sqrt{l} \left[G\eta_0^2 z_{\text{eq}} \ln \left(\frac{z_{\text{in}}}{z_{\text{eq}}} \right) \right] \frac{\Pi^{(T)}(k)}{k\eta_0} \left\{ \left[1 - \frac{l^2}{2(k\eta_0)^2} \right] J_{l+3}(k\eta_0) + \frac{J_{l+4}(k\eta_0)}{k\eta_0} \right\}. \quad (6.24)$$

Substituting Eq. (6.24) into Eq. (6.1) and using Eq. (2.22), we obtain

$$\begin{aligned} C_l^{EE(T)} &= \frac{49}{40000} (2\pi)^{2n+12} l \left[G\eta_0^2 z_{\text{eq}} \ln \left(\frac{z_{\text{in}}}{z_{\text{eq}}} \right) \right]^2 \frac{B_\lambda^4 \eta_0}{\Gamma^2 \left(\frac{n+3}{2} \right) (2n+3)} \frac{(k_D \eta_0)^{2n+3}}{(k_\lambda \eta_0)^{2n+6}} \\ &\times \int_0^{k_D} dk \left[1 + \frac{n}{n+3} \left(\frac{k}{k_D} \right)^{2n+3} \right] \left\{ \left[1 - \frac{l^2}{2(k\eta_0)^2} \right] J_{l+3}(k\eta_0) + \frac{J_{l+4}(k\eta_0)}{k\eta_0} \right\}^2. \end{aligned} \quad (6.25)$$

Note that $(2\pi)^{2n+10} B_\lambda^4 / [\Gamma^2 \left(\frac{n+3}{2} \right) k_\lambda^{2n+6}] \propto A^2$, where A is the normalization of the magnetic power spectrum in Eq. (2.5). For $n > -3/2$, using Eqs. (5.8) and (5.13) and keeping only the highest-order terms in l gives

$$l^2 C_l^{EE(T)} = \frac{49}{20000} (2\pi)^{2n+11} \left[G\eta_0^2 z_{\text{eq}} \ln \left(\frac{z_{\text{in}}}{z_{\text{eq}}} \right) \right]^2 \frac{B_\lambda^4 l^3}{\Gamma^2 \left(\frac{n+3}{2} \right) (2n+3)} \frac{(k_D \eta_0)^{2n+3}}{(k_\lambda \eta_0)^{2n+6}} \left[\ln \left(\frac{k_D \eta_0}{l} \right) - \frac{5}{6} \right], \quad n > -3/2. \quad (6.26)$$

For $-3 < n < -3/2$, using Eqs. (5.13) and (5.14) and keeping only the highest-order terms in l , we obtain

$$\begin{aligned} l^2 C_l^{EE(T)} &= 2^{2n-7} \frac{49}{625} (2\pi)^{2n+12} \left[G\eta_0^2 z_{\text{eq}} \ln \left(\frac{z_{\text{in}}}{z_{\text{eq}}} \right) \right]^2 \frac{\Gamma(-2n-3)}{\Gamma^2(-n-1)\Gamma^2 \left(\frac{n+3}{2} \right)} \frac{B_\lambda^4 (4n^2+3)}{(2n+3)(n+1)(n+3)} \left(\frac{l}{k_\lambda \eta_0} \right)^{2n+6}, \\ &-3 < n < -3/2. \end{aligned} \quad (6.27)$$

From the properties of radial functions, Hu and White place upper bounds on how fast various power spectra can grow with l (see Eq. (78) of [59]). In particular, tensor polarization power spectra can grow no faster than $l^2 C_l^{EE, BB(T)} \propto l^2$. Our results for the tensor E- and B-type (Sec. VIB 2) polarization power spectra seem to violate this constraint for $n > -2$ by an additional factor of l , which arises from numerical approximations as in the second line of Eq. (5.23). Within the tensor integral solutions of Eqs. (5.22), (6.23), and (6.30), we have to evaluate integrals of the form $\int_0^{x_0} dx [j_2(x)/x][j_l(x_0-x)/(x_0-x)^p]$. The piece $j_2(x)/x$ comes from the gravitational wave solution \dot{h} of Eq. (4.21) whereas the piece $j_l(x_0-x)/(x_0-x)^p$ comes from the radial functions. In Ref. [59], only the radial function properties are used to determine the upper bounds on the power spectra growth rate, whereas the source behavior has been entirely neglected. Our numerical approximation in Eq. (5.23) takes into account the source behavior, i.e. $j_2(x)/x$, and this introduces an additional factor of l in the resulting power spectra. Note that besides the tensor polarization power spectra, all the remaining power spectra conform to the growth constraints given by Ref. [59].

2. B-type Polarization

The B-type polarization integral solution for tensor perturbations is [59]

$$\frac{B_l^{(T)}(\eta_0, k)}{2l+1} = -\sqrt{6} \int_0^{\eta_0} d\eta \dot{\tau} e^{-\tau} P^{(T)} \beta_l^{(T)} [k(\eta_0 - \eta)], \quad (6.28)$$

where

$$\beta_l^{(T)}(x) = \frac{1}{2} \left[j_l'(x) + 2 \frac{j_l(x)}{x} \right] \quad (6.29)$$

is the tensor B-type polarization radial function. Using Eqs. (5.20), (4.21) and (6.5), and defining $x \equiv k\eta$ and $x_0 \equiv k\eta_0$, we approximate the tensor B-type polarization integral solution as

$$\frac{B_l^{(T)}(\eta_0, k)}{2l+1} \simeq \frac{\sqrt{6}}{3} (2\pi) \left[G\eta_0^2 z_{\text{eq}} \ln \left(\frac{z_{\text{in}}}{z_{\text{eq}}} \right) \right] \Pi^{(T)}(k) \int_0^{x_0} dx \frac{j_2(x)}{x} \left[(l+2) \frac{j_l(x_0 - x)}{x_0 - x} - j_{l+1}(x_0 - x) \right]. \quad (6.30)$$

A similar manipulation as in Eq. (5.23) gives

$$\frac{B_l^{(T)}(\eta_0, k)}{2l+1} \simeq \frac{7}{100} (2\pi)^2 \sqrt{l} \left[G\eta_0^2 z_{\text{eq}} \ln \left(\frac{z_{\text{in}}}{z_{\text{eq}}} \right) \right] \frac{\Pi^{(T)}(k)}{k\eta_0} \left[l \frac{J_{l+3}(k\eta_0)}{k\eta_0} - J_{l+4}(k\eta_0) \right]. \quad (6.31)$$

Substituting Eq. (6.31) into (6.2) and using Eq. (2.22), we obtain

$$\begin{aligned} C_l^{BB(T)} &= \frac{49}{40000} (2\pi)^{2n+12} l \left[G\eta_0^2 z_{\text{eq}} \ln \left(\frac{z_{\text{in}}}{z_{\text{eq}}} \right) \right]^2 \frac{B_\lambda^4 \eta_0}{\Gamma^2 \left(\frac{n+3}{2} \right) (2n+3)} \frac{(k_D \eta_0)^{2n+3}}{(k_\lambda \eta_0)^{2n+6}} \\ &\quad \times \int_0^{k_D} dk \left[1 + \frac{n}{n+3} \left(\frac{k}{k_D} \right)^{2n+3} \right] \left[l \frac{J_{l+3}(k\eta_0)}{k\eta_0} - J_{l+4}(k\eta_0) \right]^2. \end{aligned} \quad (6.32)$$

Note that $(2\pi)^{2n+10} B_\lambda^4 / [\Gamma^2 \left(\frac{n+3}{2} \right) k_\lambda^{2n+6}] \propto A^2$, where A is the normalization of the magnetic power spectrum in Eq. (2.5). For $n > -3/2$, using Eqs. (5.8) and (5.13), we obtain

$$l^2 C_l^{BB(T)} = \frac{49}{20000} (2\pi)^{2n+11} \left[G\eta_0^2 z_{\text{eq}} \ln \left(\frac{z_{\text{in}}}{z_{\text{eq}}} \right) \right]^2 \frac{B_\lambda^4 l^3}{\Gamma^2 \left(\frac{n+3}{2} \right) (2n+3)} \frac{(k_D \eta_0)^{2n+3}}{(k_\lambda \eta_0)^{2n+6}} \left[\ln \left(\frac{k_D \eta_0}{l} \right) - 1 \right], \quad (6.33)$$

$n > -3/2.$

For $-3 < n < -3/2$, a similar calculation gives

$$l^2 C_l^{BB(T)} = 2^{2n-4} \frac{49}{625} (2\pi)^{2n+12} \left[G\eta_0^2 z_{\text{eq}} \ln \left(\frac{z_{\text{in}}}{z_{\text{eq}}} \right) \right]^2 \frac{\Gamma(-2n-3)}{\Gamma^2(-n-1)\Gamma^2 \left(\frac{n+3}{2} \right)} \frac{-B_\lambda^4 n}{(2n+3)(n+1)(n+3)} \left(\frac{l}{k_\lambda \eta_0} \right)^{2n+6}, \quad (6.34)$$

$-3 < n < -3/2.$

VII. CROSS-CORRELATION POWER SPECTRA

Since temperature Θ_l has electric parity $(-1)^l$, only E_l couples to Θ_l in the Thomson scattering and hence $C_l^{\Theta E}$ is the only possible cross correlation. The cross-correlation power spectrum is defined similarly as the temperature and polarization power spectra:

$$C_l^{\Theta E(X)} = \frac{4}{\pi} \int dk k^2 \frac{\Theta_l^{(X)}(\eta_0, k)}{2l+1} \frac{E_l^{(X)*}(\eta_0, k)}{2l+1}, \quad (7.1)$$

where X stands for V or T .

A. Vector Cross-Correlation Power Spectra

As discussed in Ref. [59] and shown in its Fig. 5, the vector dipole radial function $j_l^{(1V)}$ does not correlate well with its E-type polarization radial function $\epsilon_l^{(V)}$ whereas its quadrupole radial function $j_l^{(2V)}$ does. Therefore to compute the vector cross-correlation power spectra, we need to retain the term proportional to $j_l^{(2V)}$ in the vector temperature integral solution, though in the calculation of the temperature power spectra, we have neglected it since it is suppressed relative to the $j_l^{(1V)}$ term.

Beginning with Eq. (5.5), retaining the $j_l^{(2V)}$ term, neglecting the vector potential, and using Eqs. (5.4) and (6.5), we arrive at the following vector temperature integral solution as in Eq. (5.6):

$$\frac{\Theta_l^{(V)}(\eta_0, k)}{2l+1} \simeq \sqrt{\frac{l(l+1)}{2}} \Omega(\eta_{\text{dec}}, k) \left\{ \frac{j_l(k\eta_0)}{k\eta_0} + \frac{kL_{\gamma \text{dec}}}{3} \left[(l-1) \frac{j_l(k\eta_0)}{(k\eta_0)^2} - \frac{j_{l+1}(k\eta_0)}{k\eta_0} \right] \right\}. \quad (7.2)$$

Substituting Eqs. (7.2) and (6.6) into (7.1) and using Eqs. (4.14) and (2.18), we obtain

$$\begin{aligned} C_l^{\Theta E(V)} = & -\frac{(2\pi)^{2n+11}}{12} \sqrt{l(l-1)(l+1)(l+2)} \left(\frac{\eta_{\text{dec}}\eta_0}{1+R_{\text{dec}}} \right)^2 \frac{v_{A\lambda}^4}{\Gamma^2\left(\frac{n+3}{2}\right)(2n+3)} \frac{(k_D\eta_0)^{2n+3}}{(k_\lambda\eta_0)^{2n+6}} \\ & \times L_{\gamma \text{dec}} \int_0^{k_S} dk k^4 \left[1 + \frac{n}{n+3} \left(\frac{k}{k_D} \right)^{2n+3} \right] \left\{ (l+1) \frac{J_{l+1/2}^2(k\eta_0)}{(k\eta_0)^3} - \frac{J_{l+1/2}(k\eta_0)J_{l+3/2}(k\eta_0)}{(k\eta_0)^2} \right. \\ & \left. + \frac{kL_{\gamma \text{dec}}}{3} \left[(l^2-1) \frac{J_{l+1/2}^2(k\eta_0)}{(k\eta_0)^4} - 2l \frac{J_{l+1/2}(k\eta_0)J_{l+3/2}(k\eta_0)}{(k\eta_0)^3} + \frac{J_{l+3/2}^2(k\eta_0)}{(k\eta_0)^2} \right] \right\}, \quad (7.3) \end{aligned}$$

where again we have neglected the contribution coming from the damped vorticity term, which is negligible ($< 3\%$) for $l \leq 500$ and all cases of n . Note that $(2\pi)^{2n+10} v_{A\lambda}^4 / [\Gamma^2\left(\frac{n+3}{2}\right) k_\lambda^{2n+6}] \propto A^2$, where A is the normalization of the magnetic power spectrum in Eq. (2.5). The first two terms within the curly bracket arise from correlating $j_l^{(1V)}$ with $\epsilon_l^{(V)}$. Although the second term proportional to $J_{l+1/2}(k\eta_0)J_{l+3/2}(k\eta_0)$ cannot be approximated analytically, a numerical evaluation however shows that these two terms always roughly cancel each other, which agrees with Ref. [59] that $j_l^{(1V)}$ does not correlate well with $\epsilon_l^{(V)}$. The remaining three terms arise from correlating $j_l^{(2V)}$ with $\epsilon_l^{(V)}$. In the limit $l \gg 1$, these terms and the three Bessel terms within the vector E-type polarization power spectrum expression of Eq. (6.7) are almost identical. To simplify the approximation, we will neglect the two terms arising from the correlation between $j_l^{(1V)}$ and $\epsilon_l^{(V)}$. Thus apart from an overall minus sign, the resulting power spectra for all cases here are approximately equal to the corresponding vector E-type polarization power spectra, given in Eqs. (6.9) and (6.11) to (6.13).

Since we have neglected two terms in the vector cross-correlation power spectrum expression of Eq. (7.3), accuracy here is worse than that of the corresponding E-type polarization power spectra. Note that the terms arising from the correlation between $j_l^{(2V)}$ and $\epsilon_l^{(V)}$ are suppressed by an additional factor of $kL_{\gamma \text{dec}}$ relative to the two terms arising from the correlation between $j_l^{(1V)}$ and $\epsilon_l^{(V)}$. Because of this suppression factor, a numerical calculation shows that the residuals of the first two neglected terms can easily be the same order as the remaining retained terms, reducing the accuracy of our approximation. Our approximation is good to within a factor of three in general and tends to underestimate.

B. Tensor Cross-Correlation Power Spectra

Using Eqs. (5.25), (6.24), and (7.1), we obtain the tensor cross-correlation power spectrum expression

$$\begin{aligned} C_l^{\Theta E(T)} = & \frac{49}{20000} (2\pi)^{2n+12} l^3 \left[G\eta_0^2 z_{\text{eq}} \ln \left(\frac{z_{\text{in}}}{z_{\text{eq}}} \right) \right]^2 \frac{B_\lambda^4}{\Gamma^2\left(\frac{n+3}{2}\right)(2n+3)\eta_0} \frac{(k_D\eta_0)^{2n+3}}{(k_\lambda\eta_0)^{2n+6}} \\ & \times \int_0^{k_D} dk k^{-2} \left[1 + \frac{n}{n+3} \left(\frac{k}{k_D} \right)^{2n+3} \right] \left\{ \left[1 - \frac{l^2}{2(k\eta_0)^2} \right] J_{l+3}^2(k\eta_0) + \frac{J_{l+3}(k\eta_0)J_{l+4}(k\eta_0)}{k\eta_0} \right\}. \quad (7.4) \end{aligned}$$

Note that $(2\pi)^{2n+10} B_\lambda^4 / [\Gamma^2\left(\frac{n+3}{2}\right) k_\lambda^{2n+6}] \propto A^2$, where A is the normalization of the magnetic power spectrum in Eq. (2.5). For $n > -3/2$, using Eq. (5.13) and keeping only the highest-order terms in l , we obtain

$$l^2 C_l^{\Theta E(T)} = \frac{49}{15000} (2\pi)^{2n+11} \left[G \eta_0^2 z_{\text{eq}} \ln \left(\frac{z_{\text{in}}}{z_{\text{eq}}} \right) \right]^2 \frac{B_\lambda^4 l^3}{\Gamma^2 \left(\frac{n+3}{2} \right) (2n+3)} \frac{(k_D \eta_0)^{2n+3}}{(k_\lambda \eta_0)^{2n+6}}, \quad n > -3/2. \quad (7.5)$$

For $-3 < n < -3/2$, a similar calculation gives

$$l^2 C_l^{\Theta E(T)} = 2^{2n-6} \frac{49}{625} (2\pi)^{2n+12} \left[G \eta_0^2 z_{\text{eq}} \ln \left(\frac{z_{\text{in}}}{z_{\text{eq}}} \right) \right]^2 \frac{\Gamma(-2n-1)}{\Gamma^2(-n) \Gamma^2 \left(\frac{n+3}{2} \right)} \frac{B_\lambda^4 (2n-1)}{(2n+3)(n+3)} \left(\frac{l}{k_\lambda \eta_0} \right)^{2n+6}, \quad -3 < n < -3/2. \quad (7.6)$$

VIII. RESULTS AND DISCUSSION

The CMB power spectra generated by a stochastic magnetic field are plotted for $l = 5$ to $l = 500$ in Figs. 1, 2, and 3. Since we are interested in the signatures of the various microwave background power spectra arising from primordial fields that are large enough to result in the observed galactic fields via adiabatic compression, for each plot, we choose the magnetic comoving mean-field amplitude to be $B_\lambda = 10^{-9}$ G and fix $\lambda = 1$ Mpc, i.e. galaxy and cluster scales. For simplicity, we consider a standard Cold Dark Matter Universe (sCDM), i.e. a flat Universe composed of only dust and radiation ($\eta_0 \simeq 6000 h^{-1}$ Mpc) with $\Omega_b = 0.05$ and $h = 0.5$. Including a possible cosmological constant will affect the scale factor evolution only relatively recently at redshift of a few and will result in a slightly larger η_0 . The magnetic power spectrum cutoff wavenumbers for vector and tensor perturbations are given by Eqs. (3.3) and (3.6) respectively. Thus for $n = -1$ and $n = 2$ for example, with $B_\lambda = 10^{-9}$ G and $\lambda = 1$ Mpc, we have $k_D \simeq 27.9$ Mpc $^{-1}$ and $k_D \simeq 14.7$ Mpc $^{-1}$ respectively for vector perturbations; whereas for tensor perturbations, we obtain $k_D \simeq 80.9$ Mpc $^{-1}$ and $k_D \simeq 27.1$ Mpc $^{-1}$ respectively. For the tensor perturbations, we assume $z_{\text{in}}/z_{\text{eq}} = 10^9$ as in Ref. [58]; the resulting fluctuations, however, depend only logarithmically on z_{in} . In our analysis, we do not decompose the magnetic field into a large homogeneous component and a small fluctuating piece. The stochastic magnetic field then affects the stress-energy tensor and hence the metric perturbations quadratically. In computing the source terms of vector and tensor perturbations [cf. Eqs. (2.18) and (2.22) respectively], convolution of the magnetic field couples the large and small scale modes, resulting in the cutoff scale perturbations completely dominate the large scale modes for $n > -3/2$. Thus for $n > -3/2$, k_D will determine the overall amplitude of the fluctuations.

Throughout the paper, we have been stating explicitly the terms that are proportional to the normalization A of the magnetic power spectrum. Any power-law magnetic field can be specified completely by the normalization A and the spectral index n . Since we are interested in constraining the primordial magnetic field strength on galaxy scales, we choose to fix B_λ and λ and determine A for each n using Eq. (2.7). If however one is interested in the CMB power spectra with A fixed, then each n will give a different value of $B_\lambda(n)$ via Eq. (2.7). Either way will not affect the final constraints for the magnetic comoving mean-field amplitude. Indeed, we find it easier to constrain the amplitude by keeping B_λ fixed.

Figure 1 shows the separate vector and tensor contributions to the CMB power spectra for four different values of n . For $n < -3/2$, the CMB power spectra do not depend on k_D , and the size of the anisotropies increases as n gets smaller; a scale-invariant magnetic field with $n = -2.99$ generates the largest anisotropies and hence it will yield the most stringent limit on the primordial magnetic field (see also Fig. 1 of [58]). For $n > -3/2$, the CMB power spectra are k_D -dependent and scale as k_D^{2n+3} ; thus more and more stringent magnetic field limits can be obtained as n increases toward causal values¹. For the vector perturbations, the BB power spectrum is slightly larger than that of the EE's, as also pointed out in Ref. [59] that the vector CMB polarization is dominated by the B-type modes; whereas the EE and ΘE power spectra are approximately identical. Naively, the ΘE cross correlation would be expected to be larger than the polarization power spectra simply because the temperature fluctuations are larger than the polarization fluctuations. However, the temperature fluctuations are dominated by the vector dipole term, which correlates poorly with the radial function describing E-type polarization. Thus the ΘE spectrum is dominated by a subdominant temperature contribution arising from the vector quadrupole term, which then coincidentally renders the spectrum a form approximately identical to the E-type polarization itself. However in reality, the ΘE spectrum can be slightly larger than the polarization spectra since our approximation is good to within a factor of three and

¹Figure 1 of Ref. [58] shows a weaker and weaker upper bound for B_λ as n increases from $-3/2$. This is because the authors there have inappropriately adopted a smoothing scale smaller than the magnetic damping scale and have employed a different value for the damping scale (see Sec. IIIB for details).

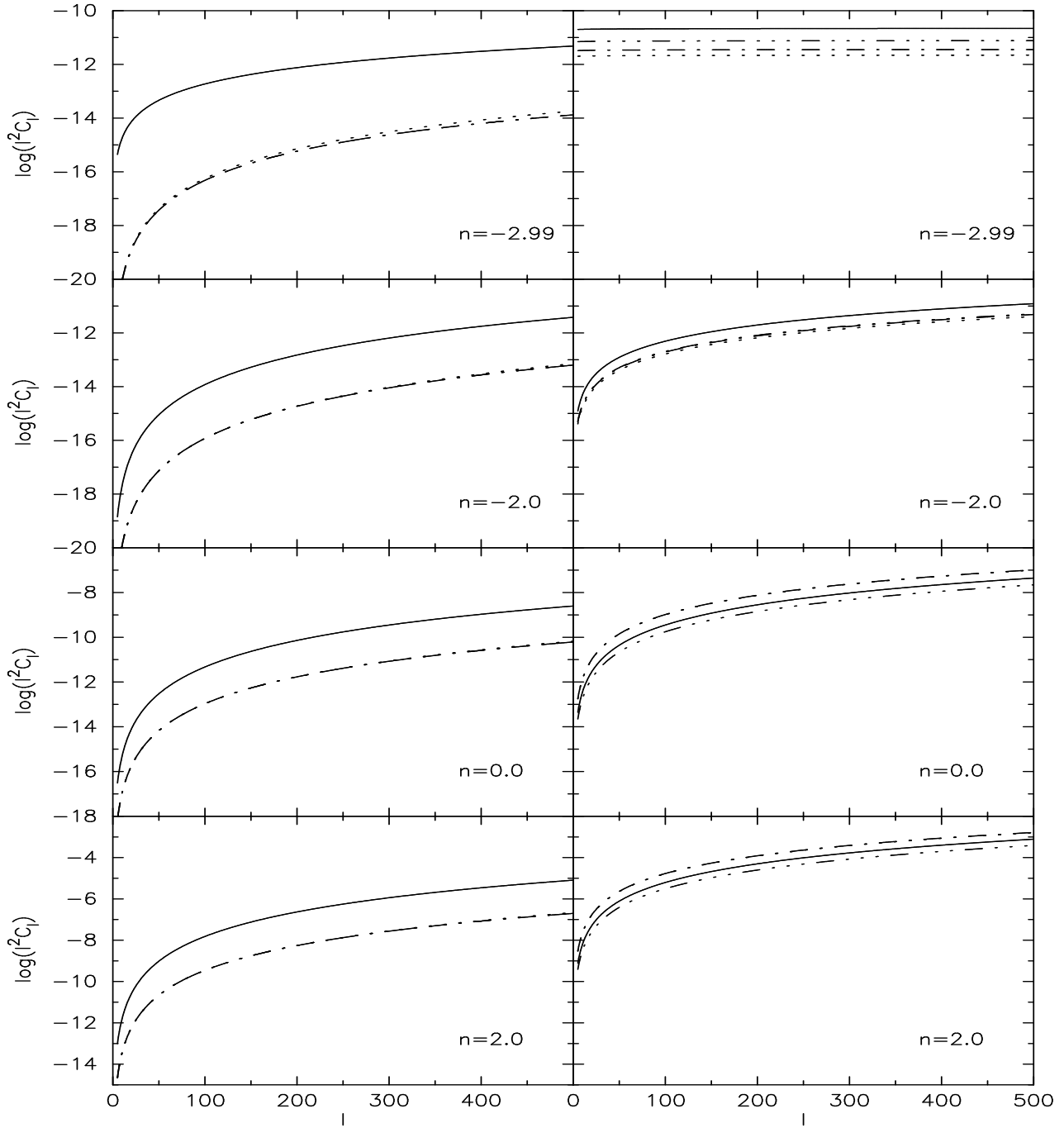


FIG. 1. The microwave background power spectra for vector (left panels) and tensor (right panels) perturbations from a power-law stochastic magnetic field with spectral index n . Solid line represents $\Theta\Theta$, dash-dot line represents EE , dotted line represents BB , and dash-dot-dot-dot line represents ΘE . The magnetic comoving mean-field amplitude is chosen to be $B_\lambda = 10^{-9}$ G, with a smoothing Gaussian sphere comoving radius of $\lambda = 1$ Mpc. The magnetic damping cutoff wavenumbers for vector and tensor perturbations are given by Eqs. (3.3) and (3.6) respectively. The absolute values of the vector cross correlations are plotted. For the tensor perturbations, we assume $z_{\text{in}}/z_{\text{eq}} = 10^9$.

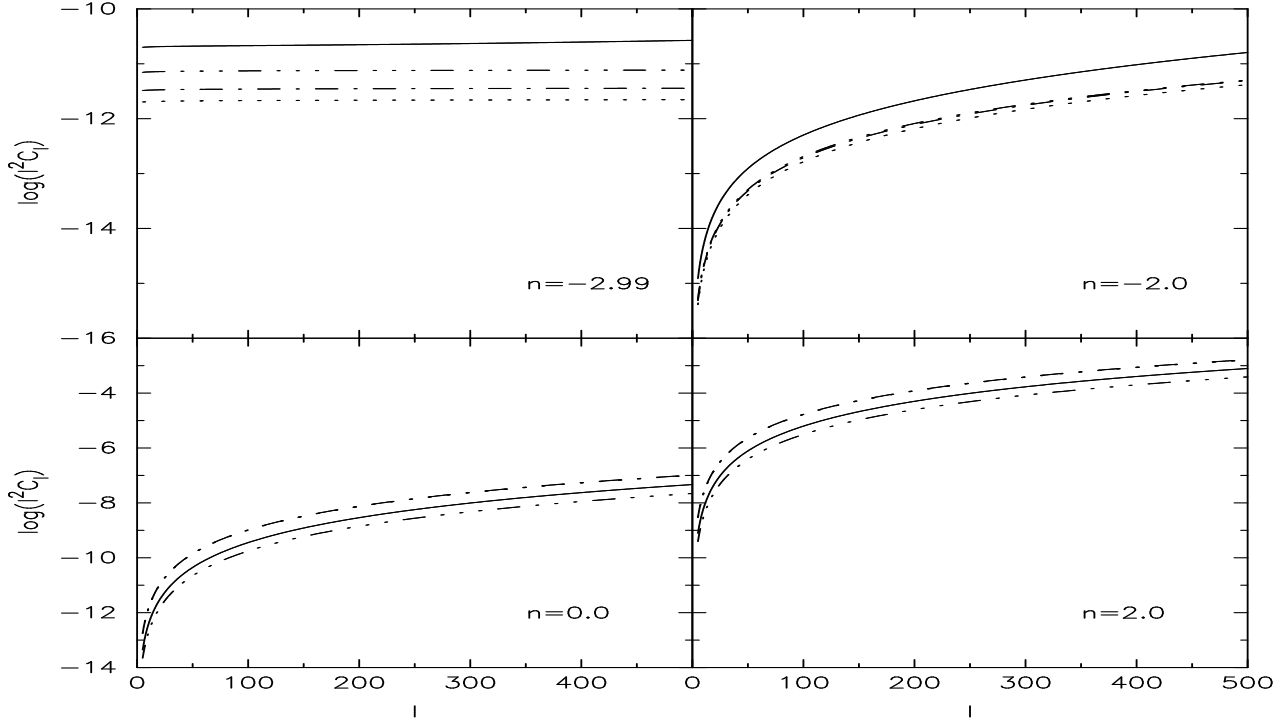


FIG. 2. Same as in Fig. 1, except that the microwave background power spectra are for vector plus tensor perturbations.

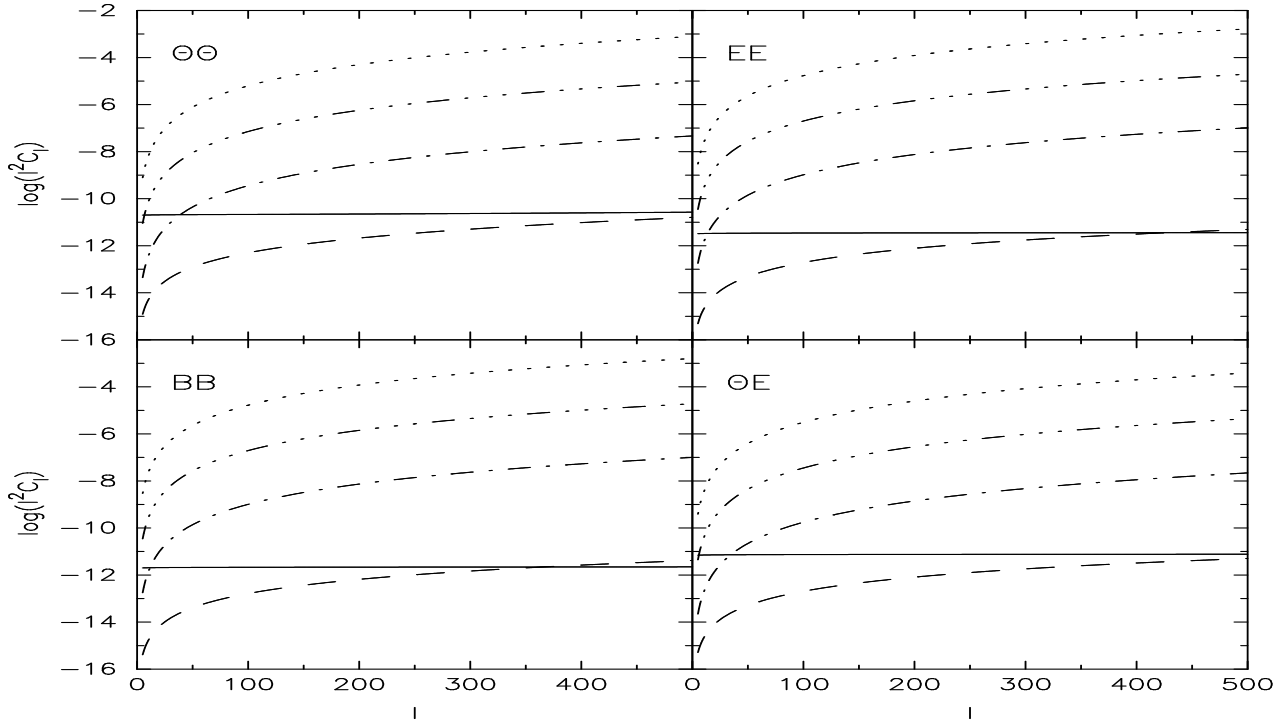


FIG. 3. Each panel shows a single power spectrum for various values of n . Solid line represents $n = -2.99$, dashed line represents $n = -2.0$, dash-dot line represents $n = 0.0$, dash-dot-dot-dot line represents $n = 1.0$, and dotted line represents $n = 2.0$.

tends to underestimate in general (see Sec. VII A). Note that while $n \rightarrow -3$ corresponds to a scale-invariant magnetic field, the vector power spectrum is not flat for this value. The reason is that the vorticity, Eq. (4.14), has an extra factor of k compared to the magnetic field itself. The vector cross correlation is always negative; its absolute value is plotted.

For the tensor perturbations, the E-type is slightly larger than the B-type polarization power spectrum. The polarization power spectra are actually comparable to the temperature power spectrum for $n > -3/2$. This is due to the additional logarithmic dependence on the magnetic damping cutoff wavenumber for the polarization power spectra [cf. Eqs. (6.26) and (6.33)], and also because both the temperature and polarization fluctuations are due to the intrinsic temperature quadrupole moments, which arise from the gravitational wave solution \dot{h} of Eq. (4.21) instead of being generated via free streaming the dipoles as in the case of the vector perturbations. Also for $n > -3/2$, the gravitational wave source term is approximately independent of k and the resulting power spectra then possess the well-known behavior of a white noise source $l^2 C_l \propto l^3$. Furthermore, since tensor perturbations are damped on scales smaller than that of the vector perturbations as discussed in Sec. III B, their induced anisotropies will then be larger than that of the vector's for $n > -3/2$ where k_D determines the overall amplitude of the microwave background power spectra. As expected, the tensor power spectrum is flat for $n \rightarrow -3$ since we have a scale-invariant magnetic field for this value. The tensor cross correlation is always positive.

The difference between the sign of the vector and tensor cross correlations can be understood from the geometric properties of the projection of their corresponding temperature and polarization sources as anisotropies on the sky [59]. The sign of the vector and tensor cross correlations is determined by respectively (cf. Eq. (80) of Ref. [59])

$$\text{sgn}[C_l^{\Theta E(V)}] = -\text{sgn}[P^{(V)}(\dot{\tau}P^{(V)})], \quad (8.1)$$

$$\text{sgn}[C_l^{\Theta E(T)}] = \text{sgn}[P^{(T)}(\dot{\tau}P^{(T)} - \dot{h})]. \quad (8.2)$$

The sign of the vector cross correlation is therefore always opposite to that of the tensor cross correlation.

Each panel in Fig. 2 shows the total vector plus tensor contributions for the various power spectra for a particular value of n . Each panel in Fig. 3 replots one of the four power spectra for a range of spectral indices n . As the spectral index becomes greater than zero, the amplitudes become quite large. Again, this is because for $n > -3/2$, the magnetic cutoff wavenumber k_D determines the overall amplitude of the power spectra. For a scale-invariant $n \rightarrow -3$ spectral index, a magnetic comoving mean-field amplitude of $B_\lambda = 10^{-9}$ G, and a comoving smoothing scale of $\lambda = 1$ Mpc, at $l = 500$ for example, the temperature and polarization power spectra are smaller than the amplitudes as expected from scale-invariant density perturbations normalized to COBE (i.e., CMB fluctuations in “standard” cosmological models). But for $n = 0$, the temperature power spectrum is essentially a factor of 50 whereas the E-type polarization power spectrum is a factor of 10^4 larger than that expected from the scalar Λ CDM model at $l = 500$. Therefore, observational limits will be much stronger for causal fields than for scale-invariant fields.

To estimate the potential observational limits on stochastic magnetic fields, the induced microwave background anisotropies must be large enough to be disentangled from the anisotropies arising from density perturbations. Current temperature maps give power spectrum measurements with error bars on the order of 10% out to $l = 400$ for bins of width $\Delta l = 50$ [12,14]. The MAP satellite, which is already in orbit, will make temperature measurements out to around $l = 800$ and will reach the cosmic variance limit, $\Delta C_l = (l + 1/2)^{-1/2} C_l$, out to $l = 400$ [76]. By the end of the decade, and perhaps within five years, we can expect a cosmic-variance limited temperature power spectrum measurement to $l = 3000$. Polarization fluctuations will also be detected soon, and the progress in their measurement will likely lag temperature fluctuations by about a decade. A rough but conservative estimate is that a magnetic-field signal which is at least 10% of the dominant density-perturbation signal will be detectable. The ultimate sensitivity in measuring the temperature power spectrum at, say, $l = 500$ will be significantly better than this, and the extent to which magnetic fields can be constrained depends more on the degeneracy of the magnetic field signal with shifts in various cosmological parameters. Basic statistical techniques for pursuing such an analysis are well-known (see, e.g., [62]) and will be considered elsewhere.

Using this crude 10% criterion, we can anticipate constraints on stochastic magnetic fields from upcoming temperature measurements (e.g., the MAP satellite, currently taking data) by simply comparing the predicted amplitude at $l = 500$ to the amplitude of current measurements, which is on the order of $l^2 C_l \simeq 10^{-9}$. We assume that the remainder of the power spectrum is used for discrimination between the signals from magnetic fields and other temperature power spectrum contributors. For the scale-invariant magnetic field with $n \rightarrow -3$, a comoving mean-field amplitude of $B_\lambda = 10^{-9}$ G gives temperature anisotropies at the level of $\sim 3\%$ of current measurements. Since for $n < -3/2$, $l^2 C_l \propto B_\lambda^4$, the constraint from temperature perturbations on a comoving 1 Mpc scale will be around 1.4×10^{-9} G, which is approximately at the same level as the previous constraints for a primordial homogeneous magnetic field [44–46]. The addition of E-type polarization measurements here will improve the constraint, since the ratio of the E-type polarization to temperature power spectra is larger for stochastic magnetic fields than the

dominant density perturbations. For $n > -3/2$, the polarization power spectra are comparable to the temperature power spectrum due to the dominant tensor perturbations; thus E-type polarization measurements will yield more stringent constraints than temperature measurements alone. Here we will be conservative and project stochastic magnetic field constraints using temperature measurements only. For $n > -3/2$, we have $l^2 C_l \propto B_\lambda^{14/(n+5)}$, where $14/(n+5) = 4 + [-2/(n+5)](2n+3)$, since $l^2 C_l \propto A^2 k_D^{2n+3}$, $A \propto B_\lambda^2$ [cf. Eq. (2.7)], and $k_D \propto B_\lambda^{-2/(n+5)}$ [cf. Eqs. (3.3) and (3.6)]. As n increases towards causal values, the amplitude of the temperature fluctuations increases as k_D^{2n+3} and hence the constraints become stronger. At $n = 0$, $l^2 C_l$ at $l = 500$ is approximately 5×10^{-8} , which will yield a constraint on B_λ of $\left(\frac{5 \times 10^{-8}}{0.1 \times 10^{-9}}\right)^{-5/14} \times 10^{-9} \text{ G} \simeq 10^{-10} \text{ G}$. For the causal field $n = 2$, the constraint on B_λ will be as small as $4 \times 10^{-13} \text{ G}$. Such constraints will be stronger than any current limits on Mpc-scale primordial stochastic magnetic fields at decoupling.

Ultimately, B-type polarization has the greatest potential for constraining primordial magnetic fields. This is a cleaner signature, because primordial scalar (density) perturbations produce none [60,74]. Aside from polarized foreground emission, the only other expected sources are from primordial tensor perturbations and from gravitational lensing [63]. Tensor perturbations with a spectrum near scale-invariant will give significant anisotropies only at large angular scales ($l < 100$), while lensing contributes mainly at small angular scales ($l > 500$). Stochastic magnetic fields will contribute on intermediate scales and should be clearly distinguishable. If foreground emission can be separated from its frequency dependence, limits on B_λ from B-type polarization should be determined purely by measurement error bars on C_l^{BB} . Note that a primordial magnetic field also generates an additional B-type polarization signal via Faraday rotation of the CMB polarization [47]. This signal will be negligible compared to the direct B-type polarization signal for any frequency of practical interest.

All of the results in this paper have been obtained via analytic approximations to the exact solutions. Apart from the vector cross-correlation power spectrum, the accuracy of the results is as good as the quality of the analytic approximations to various expressions, except that the vector temperature case has neglected an additional few percent temperature contribution arising from the angular dependence of polarization and the vector potential. These approximations are all discussed in the text; in sum, they are good to within 20% over the range of parameters considered, with the exception of the vector temperature case in the regime $-2.5 \leq n < -2$, which is good to within 30%. Meanwhile, accuracy of the vector cross-correlation power spectrum is only good to within a factor of three, since we have neglected the two terms in Eq. (7.3) arising from the correlation between the temperature dipole and the E-type polarization radial functions. It is important to realize that errors in these analytic approximations will have negligible effects on the estimation of the magnetic field limits for $n \leq 2$ since the amplitude of each power spectrum scales as B_λ^4 for $n < -3/2$ and $B_\lambda^{14/(n+5)}$ for $n > -3/2$.

In this paper, we have focussed on the magnetic field-induced microwave background anisotropies for $l \leq 500$, where the analysis is relatively simple and free from the detailed microphysics of recombination. We have only considered vector and tensor metric perturbations; for smaller angular scales $500 < l < 2000$, the magnetic-induced CMB anisotropies are dominated by vector perturbations [57]. Stochastic magnetic fields will also produce scalar perturbations. This case is significantly more complex due to physical compensation effects and the large number of terms involved in the relevant expressions. Rough analytic estimates show that including the scalar results will only modestly improve the magnetic field constraints given in this paper, since radiation pressure prevents the induced density fluctuations from growing effectively before recombination and the compressional modes are erased up to the Silk scale L_S [41,42]. Therefore scalar perturbations will generally give a subdominant contribution to the microwave background anisotropy.

Our results suggest that while it may be plausible for primordial stochastic fields with $n \lesssim 0$ to result in the observed galactic fields via adiabatic compression alone, it will be very difficult for causal fields without invoking some form of dynamo mechanism. In a recent paper [77], a similar calculation using the nucleosynthesis bound on gravitational radiation induced by the anisotropic stress of a primordial stochastic magnetic field yields extremely stringent limits on the galactic-scale magnetic field amplitudes ($B_\lambda \leq 10^{-27} \text{ G}$) for fields generated at the electroweak phase transition or earlier, thus ruling out most of the magnetogenesis processes for primordial fields seeding the observed large-scale coherent galactic fields.

ACKNOWLEDGMENTS

We are extremely grateful to R. Durrer for numerous explanations and invaluable comments and suggestions. W. Hu and M. White contributed other helpful discussions. The referee, Karsten Jedamzik, alerted us to inadequate treatments of vorticity and magnetic damping in an earlier version of this paper, in addition to useful discussions during its initial preparation. This work has been supported by the COBASE program of the U.S. National Research

Council and by the NASA Astrophysics Theory Program through grant NAG5-7015. A.K. is a Cotrell Scholar of the Research Corporation. T.K. acknowledges the kind hospitality of Rutgers University.

APPENDIX A: DERIVATION OF THE VECTOR ISOTROPIC SPECTRUM

Our objective is to derive the vector isotropic spectrum $|\Pi^{(V)}(k)|^2$ defined in Eq. (2.17), which will be useful for calculating vector CMB power spectra. Using Eq. (2.14), the two-point correlation function of $\Pi_i^{(V)}$ is given by

$$\langle \Pi_i^{(V)}(\mathbf{k}) \Pi_i^{(V)*}(\mathbf{k}') \rangle = P_{ib} \hat{k}_a P'_{id} \hat{k}'_c \langle \tau_{ab}^{(B)}(\mathbf{k}) \tau_{cd}^{(B)*}(\mathbf{k}') \rangle, \quad (\text{A1})$$

where $P'_{id} = \delta_{id} - \hat{k}'_i \hat{k}'_d$. We simplify our calculation by splitting the electromagnetic stress-energy tensor into two pieces: $\tau_{ij}^{(B)}(\mathbf{k}) = \tau_{ij}^{(B,1)}(\mathbf{k}) + \tau_{ij}^{(B,2)}(\mathbf{k})$ where

$$\tau_{ij}^{(B,1)}(\mathbf{k}) \equiv \frac{1}{(2\pi)^3} \frac{1}{4\pi} \int d^3p B_i(\mathbf{p}) B_j(\mathbf{k} - \mathbf{p}), \quad (\text{A2a})$$

$$\tau_{ij}^{(B,2)}(\mathbf{k}) \equiv -\frac{1}{(2\pi)^3} \frac{1}{8\pi} \delta_{ij} \int d^3p B_l(\mathbf{p}) B_l(\mathbf{k} - \mathbf{p}). \quad (\text{A2b})$$

The two-point correlation function of the electromagnetic stress-energy tensor in Eq. (A1) will now be described by a sum of four two-point correlation functions:

$$\begin{aligned} \langle \tau_{ab}^{(B)}(\mathbf{k}) \tau_{cd}^{(B)*}(\mathbf{k}') \rangle &= \langle \tau_{ab}^{(B,1)}(\mathbf{k}) \tau_{cd}^{(B,1)*}(\mathbf{k}') \rangle + \langle \tau_{ab}^{(B,1)}(\mathbf{k}) \tau_{cd}^{(B,2)*}(\mathbf{k}') \rangle \\ &\quad + \langle \tau_{ab}^{(B,2)}(\mathbf{k}) \tau_{cd}^{(B,1)*}(\mathbf{k}') \rangle + \langle \tau_{ab}^{(B,2)}(\mathbf{k}) \tau_{cd}^{(B,2)*}(\mathbf{k}') \rangle. \end{aligned} \quad (\text{A3})$$

Only $\langle \tau_{ab}^{(B,1)} \tau_{cd}^{(B,1)*} \rangle$ above has a non-vanishing contribution toward the two-point correlation function of $\Pi_i^{(V)}$ in Eq. (A1), since each of the remaining correlation functions in Eq. (A3) contains either δ_{ab} , δ_{cd} , or both, and will vanish when they are acted upon by $P_{ib} \hat{k}_a P'_{id} \hat{k}'_c$. We can now rewrite Eq. (A1) as

$$\langle \Pi_i^{(V)}(\mathbf{k}) \Pi_i^{(V)*}(\mathbf{k}') \rangle = P_{ib} \hat{k}_a P'_{id} \hat{k}'_c \langle \tau_{ab}^{(B,1)}(\mathbf{k}) \tau_{cd}^{(B,1)*}(\mathbf{k}') \rangle. \quad (\text{A4})$$

We can evaluate the two-point correlation function $\langle \tau_{ab}^{(B,1)} \tau_{cd}^{(B,1)*} \rangle$ as follows. Beginning with the definition of Eq. (A2a), we assume the random magnetic field is Gaussian and apply Wick's theorem

$$\begin{aligned} \langle B_i(\mathbf{k}_i) B_j(\mathbf{k}_j) B_l(\mathbf{k}_l) B_m(\mathbf{k}_m) \rangle &= \langle B_i(\mathbf{k}_i) B_j(\mathbf{k}_j) \rangle \langle B_l(\mathbf{k}_l) B_m(\mathbf{k}_m) \rangle + \langle B_i(\mathbf{k}_i) B_l(\mathbf{k}_l) \rangle \langle B_j(\mathbf{k}_j) B_m(\mathbf{k}_m) \rangle \\ &\quad + \langle B_i(\mathbf{k}_i) B_m(\mathbf{k}_m) \rangle \langle B_j(\mathbf{k}_j) B_l(\mathbf{k}_l) \rangle \end{aligned} \quad (\text{A5})$$

and the reality condition $B_i^*(\mathbf{k}) = B_i(-\mathbf{k})$, and finally use Eq. (2.1) for the form of the stochastic magnetic field two-point correlation function to arrive at (see also [58])

$$\begin{aligned} \langle \tau_{ab}^{(B,1)}(\mathbf{k}) \tau_{cd}^{(B,1)*}(\mathbf{k}') \rangle &= \frac{1}{(4\pi)^2} \int d^3p P(p) P(|\mathbf{k} - \mathbf{p}|) [(\delta_{ac} - \hat{p}_a \hat{p}_c) (\delta_{bd} - (\widehat{\mathbf{k} - \mathbf{p}})_b (\widehat{\mathbf{k} - \mathbf{p}})_d) \\ &\quad + (\delta_{ad} - \hat{p}_a \hat{p}_d) (\delta_{bc} - (\widehat{\mathbf{k} - \mathbf{p}})_b (\widehat{\mathbf{k} - \mathbf{p}})_c)] \delta(\mathbf{k} - \mathbf{k}'). \end{aligned} \quad (\text{A6})$$

Substitute Eq. (A6) into Eq. (A4) and define $\gamma \equiv \hat{\mathbf{k}} \cdot \hat{\mathbf{p}}$, $\beta \equiv \hat{\mathbf{k}} \cdot (\widehat{\mathbf{k} - \mathbf{p}})$, and $\mu \equiv \hat{\mathbf{p}} \cdot (\widehat{\mathbf{k} - \mathbf{p}})$ to obtain the two-point correlation function of the vector $\Pi_i^{(V)}$:

$$\langle \Pi_i^{(V)}(\mathbf{k}) \Pi_i^{(V)*}(\mathbf{k}') \rangle = \frac{1}{(4\pi)^2} \int d^3p P(p) P(|\mathbf{k} - \mathbf{p}|) [(1 - \gamma^2)(1 + \beta^2) + \gamma\beta(\mu - \gamma\beta)] \delta(\mathbf{k} - \mathbf{k}'). \quad (\text{A7})$$

The integral above is similar to the mode-coupling integral $I^2(k)$ in Eq. (11) of Ref. [56]. Although it cannot be evaluated analytically, terms within the square bracket are products of cosine factors; hence the square bracket itself can be approximated by unity, which has essentially been done in Ref. [58]. Comparing with Eq. (2.17) gives

$$|\Pi^{(V)}(k)|^2 \simeq \frac{1}{8(2\pi)^2} \int d^3p P(p) P(|\mathbf{k} - \mathbf{p}|). \quad (\text{A8})$$

Using the expression for $P(k)$ in Sec. II and choosing $\hat{\mathbf{k}}$ to be the polar axis, the vector isotropic spectrum becomes

$$|\Pi^{(V)}(k)|^2 \simeq \frac{(2\pi)^{2n+9}}{32} \frac{B_\lambda^4}{\Gamma^2\left(\frac{n+3}{2}\right) k_\lambda^{2n+6}} \int_0^{k_D} dp p^{n+2} \int_{-1}^1 d\gamma (k^2 + p^2 - 2kp\gamma)^{n/2}. \quad (\text{A9})$$

The integral over γ is

$$\int_{-1}^1 d\gamma (k^2 + p^2 - 2kp\gamma)^{n/2} = \frac{1}{kp(n+2)} [(k+p)^{n+2} - |k-p|^{n+2}], \quad (\text{A10})$$

and the expression within the square bracket above can be approximated as

$$(k+p)^{n+2} - |k-p|^{n+2} \simeq \begin{cases} 2(n+2)k^{n+1}p, & p < k; \\ 2(n+2)kp^{n+1}, & \text{otherwise.} \end{cases} \quad (\text{A11})$$

Substituting Eqs. (A10) and (A11) into Eq. (A9) and evaluating, we finally arrive at the expression for the vector isotropic spectrum, Eq. (2.18).

- [1] P.P. Kronberg, Rep. Prog. Phys. **57**, 325 (1994).
- [2] K.T. Kim, P.P. Kronberg, and P.C. Tribble, Astrophys. J. **379**, 80 (1991).
- [3] Ya.B. Zeldovich, A.A. Ruzmaikin, and D.D. Sokoloff, *Magnetic Fields in Astrophysics* (Gordon and Breach, New York, 1983).
- [4] E.N. Parker, *Cosmical Magnetic Fields* (Oxford University Press, Oxford, 1979).
- [5] J.H. Piddington, Mon. Not. R. Astron. Soc. **128**, 345 (1964).
- [6] T. Ohki, M. Fujimoto, Z. Hitotuyanagi, Prog. Theor. Phys. Suppl. **31**, 77 (1964).
- [7] R.M. Kulsrud, *Galactic and Intergalactic Magnetic Fields*, edited by R. Beck, P.P. Kronberg, and R. Wielebinski (Dordrecht, Kluwer, 1990).
- [8] A. Davis, M. Lilley, and O. Törnqvist, Phys. Rev. D **60**, 021301 (1999).
- [9] B.P. Schmidt et al., Astrophys. J. **507**, 46 (1998).
- [10] S. Perlmutter et al., Astrophys. J. **517**, 565 (1999).
- [11] A.D. Miller et al., Astrophys. J. Lett. **524**, L1 (1999).
- [12] S. Hanany et al., Astrophys. J. Lett. **545**, L5 (2000).
- [13] A. Balbi et al., Astrophys. J. Lett. **545**, L1 (2000).
- [14] P. de Bernardis et al., Nature, **404**, 955 (2000).
- [15] A.E. Lange et al., Phys. Rev. D **63**, 042001 (2001).
- [16] C.M. Ko and E.N. Parker, Astrophys. J. **341**, 828 (1989).
- [17] S.I. Vainshtein and R. Rosner, Astrophys. J. **376**, 199 (1991).
- [18] R.M. Kulsrud and S.W. Anderson, Astrophys. J. **396**, 606 (1992).
- [19] F. Cattaneo, Astrophys. J. **434**, 200 (1994).
- [20] A.V. Gruzinov and P.H. Diamond, Phys. Rev. Lett. **72**, 1651 (1994).
- [21] E. Blackman, Phys. Rev. Lett. **77**, 2694 (1996).
- [22] R. Kulsrud, S.C. Cowley, A.V. Gruzinov, and R.N. Sudan, Phys. Rep. **283**, 213 (1997).
- [23] K. Subramanian, Phys. Rev. Lett. **83**, 2957 (1999).
- [24] M.S. Turner and L.M. Widrow, Phys. Rev. D **37**, 2743 (1988).
- [25] S.M. Carroll and G.B. Field, Phys. Rev. D **43**, 3789 (1991).
- [26] W.D. Garretson, G.B. Field, and S.M. Carroll, Phys. Rev. D **46**, 5346 (1992).
- [27] B. Ratra, Astrophys. J. Lett. **391**, L1 (1992).
- [28] M. Gasperini, M. Giovannini, and G. Veneziano, Phys. Rev. Lett. **75**, 3796 (1995).
- [29] M. Gasperini, M. Giovannini, and G. Veneziano, Phys. Rev. D **52**, 6651 (1995).
- [30] T. Vachaspati, Phys. Lett. B **265**, 258 (1991).
- [31] K. Enqvist and P. Olesen, Phys. Lett. B **319**, 178 (1993).
- [32] J. Quashnock, A. Loeb, and D.N. Spergel, Astrophys. J. Lett. **344**, L49 (1989).
- [33] B. Cheng and A. Olinto, Phys. Rev. D **50**, 2421 (1994).
- [34] A.D. Dolgov and J. Silk, Phys. Rev. D **47**, 3144 (1993).
- [35] K. Enqvist and P. Olesen, Phys. Lett. B **329**, 195 (1994).

- [36] D. Grasso and H.R. Rubinstein, Phys. Rep. **348**, 163 (2001).
- [37] I. Wasserman, Astrophys. J. **224**, 337 (1978).
- [38] E.-J. Kim, A.V. Olinto, and R. Rosner, Astrophys. J. **468**, 28 (1996).
- [39] C.G. Tsagas and J.D. Barrow, Class. Quantum Grav. **14**, 2539 (1997).
- [40] C.G. Tsagas and R. Maartens, Phys. Rev. D **61**, 083519 (2000).
- [41] K. Jedamzik, V. Katalinić, and A.V. Olinto, Phys. Rev. D **57**, 3264 (1998).
- [42] K. Subramanian and J.D. Barrow, Phys. Rev. D **58**, 083502 (1998).
- [43] K. Jedamzik, V. Katalinić, and A.V. Olinto, Phys. Rev. Lett. **85**, 700 (2000).
- [44] J.D. Barrow, P.G. Ferreira, and J. Silk, Phys. Rev. Lett. **78**, 3610 (1997).
- [45] J. Adams, U.H. Danielsson, D. Grasso, and H. Rubinstein, Phys. Lett. B **388**, 253 (1996).
- [46] R. Durrer, T. Kahniashvili, and A. Yates, Phys. Rev. D **58**, 123004 (1998).
- [47] A. Kosowsky and A. Loeb, Astrophys. J. **469**, 1 (1996).
- [48] E.S. Scannapieco and P.G. Ferreira, Phys. Rev. D **56**, 7493 (1997).
- [49] D.D. Harari, J.D. Hayward, and M. Zaldarriaga, Phys. Rev. D **55**, 1841 (1997).
- [50] J.W. Dreher, C.L. Carilli, and R.A. Perley, Astrophys. J. **316**, 611 (1987).
- [51] R.A. Perley and G.B. Taylor, Astron. J. **101**, 1623 (1991).
- [52] G.B. Taylor and R.A. Perley, Astrophys. J. **416**, 554 (1993).
- [53] J.P. Ge and F.N. Owen, Astron. J. **105**, 778 (1993).
- [54] S. Koh and C.H. Lee, preprint astro-ph/0006357 (2000).
- [55] D. Lemoine, *Cosmic Microwave Background Anisotropies Generated by a Primordial Magnetic Field*, Ph.D. Thesis (1995).
- [56] K. Subramanian and J.D. Barrow, Phys. Rev. Lett. **81**, 3575 (1998).
- [57] T.R. Seshadri and K. Subramanian, Phys. Rev. Lett. **87**, 101301 (2001).
- [58] R. Durrer, P.G. Ferreira, and T. Kahniashvili, Phys. Rev. D **61**, 043001 (2000).
- [59] W. Hu and M. White, Phys. Rev. D **56**, 596 (1997).
- [60] M. Kamionkowski, A. Kosowsky, and A. Stebbins, Phys. Rev. Lett. **78**, 2058 (1997).
- [61] U. Seljak and M. Zaldarriaga, Phys. Rev. Lett. **78**, 2054 (1997).
- [62] M. Kamionkowski and A. Kosowsky, Phys. Rev. D **57**, 685 (1998).
- [63] M. Zaldarriaga and U. Seljak, Phys. Rev. D **58**, 023003 (1998).
- [64] J. Ahonen and K. Enqvist, Phys. Lett. B **382**, 40 (1996).
- [65] J.A. Peacock, *Cosmological Physics* (Cambridge University, Cambridge, 1999).
- [66] L.F. Abbott and R.K. Schaefer, Astrophys. J. **308**, 546 (1986).
- [67] P. Coles and F. Lucchin, *Cosmology: The Origin and Evolution of Cosmic Structure* (Wiley, Chichester, 1995).
- [68] J.D. Jackson, *Classical Electrodynamics* (Wiley, New York, 1975).
- [69] V.F. Mukhanov, H.A. Feldman, and R.H. Brandenberger, Phys. Rep. **215**, 203 (1992).
- [70] J.M. Bardeen, Phys. Rev. D **22**, 1882 (1980).
- [71] R. Durrer, Fundam. Cosm. Phys. **15**, 209 (1994).
- [72] M. Abramowitz and I. Stegun, *Handbook of Mathematical Functions* (Dover, New York, 1972).
- [73] I.S. Gradshteyn and I.M. Ryzhik, *Table of Integrals, Series, and Products*, edited by A. Jeffrey (Academic, San Diego, 1994).
- [74] M. Zaldarriaga and U. Seljak, Phys. Rev. D **55**, 1830 (1997).
- [75] M. Kamionkowski, A. Kosowsky, and A. Stebbins, Phys. Rev. D **55**, 7368 (1997).
- [76] See the MAP home page, URL <http://map.gsfc.nasa.gov>.
- [77] C. Caprini and R. Durrer, Phys. Rev. D **65**, 023517 (2002).